DYNAMICS OF HARVESTED RESOURCES, WITH EMPHASIS ON COMMERCIALLY EXPLOITED FISHERIES

by

Michael Crone
A Dissertation
Submitted to the
Graduate Faculty
of
George Mason University
in Partial Fulfillment of
The Requirements for the Degree
of
Doctor of Philosophy
Mathematics

Committee:

_____	Dr. Evelyn Sander, Dissertation Director
_____	Dr. Robert Axtell, Committee Member
_____	Dr. Flavia Colonna, Committee Member
_____	Dr. Maria Emelianenko, Committee Member
_____	Dr. David Walnut, Department Chairperson
_____	Dr. Donna M. Fox, Associate Dean, Office of Student Affairs & Special Programs, College of Science
_____	Dr. Peggy Agouris, Dean, College of Science
Date: _____	Spring Semester 2015 George Mason University Fairfax, VA

Dynamics of Harvested Resources, with Emphasis on Commercially Exploited Fisheries

A dissertation submitted in partial fulfillment of the requirements for the degree of Doctor of Philosophy at George Mason University

By

Michael Crone
Master of Science
University of Wyoming, 1996
Bachelor of Arts
Whitworth University, 1992

Director: Dr. Evelyn Sander, Professor
Department of Mathematics

Spring Semester 2015
George Mason University
Fairfax, VA

Dedication

I dedicate this dissertation to guinea fowl. Loud, crazy looking, and uncontrollable: you are the punk rockers of agricultural birds.

Acknowledgments

In academic work, one is always learning and building on the work of others. This thesis would not have been possible without the work of others too numerous to name, but there are a few whose help is of particular note. I would like to thank my graduate committee: Evelyn Sander, Robert Axtell, Flavia Colonna, and Maria Emelianenko for their support and advice. I would like to thank Kim DeMutsert and Kristy Lewis for sharing their expertise about the oyster and black drum system in Louisiana. I would also like to thank Elizabeth Crone for providing me background and advice on statistics in population ecology, Igor Griva for his training in optimization and AMPL and the people of Saint Paul Island, Alaska, especially Aquilina Lestenkof, for sharing their hospitality and local knowledge of marine ecology in my many visits over a period that has stretched out to more than a decade. Last, but not in any way least, I would like to thank the Aleut Community of Saint Paul, the National Oceanographic and Atmospheric Administration and the Pribilof School District for providing lodging during my stays in Saint Paul Island. Any credit must be shared with all of these people. Any errors or omissions are entirely my own.

Table of Contents

List of Tables

List of Figures

Abstract

DYNAMICS OF HARVESTED RESOURCES, WITH EMPHASIS ON COMMERCIALLY EXPLOITED FISHERIES

Michael Crone, PhD

George Mason University, 2015

Dissertation Director: Dr. Evelyn Sander

Modeling the dynamics of commercial fisheries is an active field at the crossroads of mathematics, ecology, and economics. Population levels are one of the most basic statistics used for all conservation. In all natural resource management, predictions for future populations are required to predict the impacts of management strategies. Collapses of commercial fish stocks have been reported in many regions [10, 21, 36]. Accurate understanding of both ecological and behavioral responses to commercial exploitation in fisheries is an important tool to combat population collapse. In this dissertation, we study two population models with applications in commercial fisheries. First, we study the ratio-dependent predator-prey model with constant harvests, a continuous model that has been proposed, but for which previous analysis has not been conducted. We explore the dynamics of the model in general, and then conduct a search for limit cycles that persist when the predator harvest changes. We find that stable, persistent limit cycles are not very common, especially when there is also a harvest of the prey species. We apply the model to the oyster and black drum system in Louisiana and find that a variety of parameters show a near-best fit, a track of increasing oyster populations to a level some 20-50% higher than its 23-year average. Next, we study a new discrete model that we created. This model seeks to predict harvest changes in a

tractable way, and we provide stability analysis of the model. We expand the model to incorporate several agents and apply the model from several initial conditions where overfishing is occurring. We then propose a simple management rule that, in our simulations, improves performance of the model.

Chapter 1: Introduction

In this thesis, we study two population models with applications in commercial fisheries. In this introductory chapter, we provide a background of population modeling in fisheries and ecology, with specific emphasis on where the models in this thesis draw on and fit into previous work.

In Chapter 2, we discuss a model with predator-prey interaction. A very early predator-prey model was created by Lotka and Volterra independently in the early 20^{th} century [43, 49]:

$$\dot{x} = ax - bxy$$

$$\dot{y} = cxy - dx.$$

In this model, a, b, c and d are positive constants, x represents the prey species, and y the predator species. The prey grow exponentially in the absence of predators, and the predators decay exponentially in the absence of prey. The term xy models interaction between predator and prey. Most now believe that xy is not a realistic formula for predator-prey interaction, and we are not aware of any current research uses of the entire model. However, exponential decay for the predators is still in use today and we retain it in our study.

Lotka and Volterra inspired a general class of models:

$$\dot{x} = g(x) - yf(x, y)$$

$$\dot{y} = -h(y) + cyf(x, y),$$

where c is a positive constant, $g(x)$ describes the growth or decay of the prey species in

the absence of predators, $-h(y)$ represents the growth of the predators in the absence of prey (with the minus sign in front because there is generally assumed to be decay in the absence of prey), and $yf(x, y)$ represents the interaction of predators and prey. The notation represents the fact that in most early models and, in fact, most models currently employed today, $f(x, y)$ is a function of x alone in this form, a condition known as prey dependence. The term $f(x, y)$ is known in the field as the functional response of predators to prey. As we will discuss below, the model we analyze in Chapter 2 is ratio dependent, rather than prey dependent. However, due to the prevalent use of prey dependence, we will discuss some of the various prey dependent models and their inspiration.

The functional response $f(x, y)$ is the predation rate per predator. In the Lotka-Volterra model, the predation rate per predator is bx, that is, each individual predator eats a consistent proportion of the prey population, no matter how large the prey population gets. Early adaptations to the Lotka-Volterra model involved supposing that predators become saturated ("full" in lay terminology), and the predation rate per predator as a proportion of prey declines as x gets large.

Predator saturation is an important phenomenon in ecology and affects the behavior of many species. It is well known that salmon and other migratory prey species travel in large groups to saturate their predators and help ensure that at least some of the prey survive the migration. With that in mind, it is not surprising that the original Lotka-Volterra model without saturation is not in current use. Several models were proposed with predator saturation in mind, most notably a model proposed in 1934 by Gause [30] and two models proposed in 1959 by Holling [37, 38], which came to be known as Holling I and Holling II.

Another class of models was later proposed by Holling in 1965, which include an assumption that, at some prey density levels, prey may become easier to catch in higher densities [39]. This could be the case if prey are otherwise stressed and vulnerable in high densities, or if predators have less distance to travel between each prey individual or learn how to catch prey with practice. This class of models have come to be known as Holling

III models, and some popular formulas for this situation are the ones proposed by Real in 1977 [51] and Hassell in 1978 [34].

Later work has focused on incorporating these mostly prey dependent models have been incorporated into complex computer models, such as Ecopath [25], created by the National Oceanic and Atmospheric Administration in 1992 and maintained currently by the Ecopath Research and Development Consortium, and Atlantis [29], created in 2004, a fisheries management tool developed by Fulton at the Commonwealth Scientific and Industrial Research Organisation in Australia. Both these models incorporate a multi-species food web as well as a variety of other factors including spatial features, nutrient level, age structure and migration. These models have the advantage of these incorporations when the underlying parameters are known and are a useful tool for managers in those situations. However, such models are also information intensive, in that each relationship requires one or more parameter estimates. We focus in this dissertation on a simpler abstraction: the predator-prey relationship only.

The model that we consider in this thesis is based on a model that is dependent on both prey and predator. Consider again the salmon run. Salmon run in a high density so that their predators become saturated, but predation rate per predator does not respond to the density of predators in a prey-dependent model. It seems reasonable to assume that predators would start to be crowded out from the resource, and the functional response should decline as the predator density increases. With this in mind, Arditi and Ginsberg [4] proposed a model in 1989 where the functional response was dependent on the ratio x/y of prey to predators, which has come to be known as the ratio-dependent predator-prey model. A rather comprehensive analysis of the ratio-dependent predator-prey model was conducted by Xiao and Ruan in 2001 [57]. We discuss the analysis in more detail in Chapter 2.

We are interested in modeling marine species that are commercially harvested. In 2005, Xiao and Jennings [55] analyzed an adaptation of the ratio-dependent model with a prey harvest, and, in 2006, Xiao et al [56] analyzed the ratio-dependent predator-prey model

with a commercial harvest on the predator species. The model we will study in Chapter 2 is a model with a harvest on both the predator and the prey species. To our knowledge, no such analysis is present in the literature.

Since we are also modeling fishing, we now turn our attention to other models of commercially fished species. Traditionally, fisheries models have been single species models assuming logistic growth ($\dot{x} = rx(1 - x/M)$) for the targeted species. In this model, growth is maximized at $rM/4$ when $x = M/2$ and a classic management theory known as Maximum Sustained Yield, is to attempt to stabilize the population at $M/2$ and harvest at the growth rate of $rM/4$, as this will maximize the total harvest of the population. This model is described in detail in [15]

There are a few objections to this model for deciding on a harvest. One is that the equilibrium created by this model is semi-stable, as pointed out by [15], the practical consequence being that if, due to random fluctuation or some exogenous event, x falls below $M/2$, the population will not return to equilibrium, but will continue to decline to extinction unless the harvest is reduced.

It is also argued that maximizing the harvest is not necessarily the most ecologically optimal regime. As early as 1973, Clark [15] suggested that economically optimal fishing may not imply conservation. When the discount rate (i.e., interest rate or return on investment) in the greater economy is high enough, the most economically beneficial behavior could in theory be to catch all the fish possible, up to extinction, and invest the profits in the larger economy. However, it is also true that it becomes more expensive to catch fish as their population decreases.

In 2010, Grafton et al. [31] analyzed the economics with both a discount rate and a higher catch per unit effort for higher stock biomass for four disparate fisheries and found that maximizing profits lead to a higher population than maximizing harvest for discount rates up to 10% for the slow-growing orange roughy and discount rates up to 25% for the other species considered. This set off a debate between Clark et al. [16, 17] and Grafton et al. [32]. In the end, Clark et al. [17] conclude that plausible changes in price, technology,

and/or fishing effort costs could result in extinction being economically optimal even using Grafton et al.'s model.

In Chapter 3, we study a discrete single-species model. In the absence of harvest, we model population growth by logistic growth and once again adapt the model by bringing in a commercial harvest. However, in this chapter we do not consider a constant harvest, the emphasis in Chapter 3 is on modeling a harvest that changes over time. In particular, we model the harvest as responding to changes in the harvested population in a simple way. In many sections of Chapter 3, we also consider heterogeneous agents and model them in a similar manner, but with different parameters, and observe the effect of changes in the agents.

We seek to continue work on the alignment of behavior of the individual in a way that does not impose costs on others: in economic terms, we propose to incentivize fishers to avoid negative externalities. Probably the most prominent method in fisheries of aligning these incentives is through individual transferable quotas (ITQs), which we summarize in the next few paragraphs.

A common model in economics for human behavior is that people act in their rational self-interest. Under this model, unregulated fisheries do not typically fare well. An unregulated, open-access fishery is a classic example of what is known as the tragedy of the commons. Fishers have a perverse incentive to over-exploit in the present at the expense of future resource availability because future catches are a common good, shared by all fishers, whereas current catches are a private good which the fisher does not share with others.

To counteract the tragedy of the commons, fishery managers set a total allowable catch (TAC) and fishers raced to catch fish until the TAC is reached, at which point fishing was stopped for the season. This set up a so-called derby season, where fishers raced to catch the most fish in the shortest amount of time, which has been linked to a fishing fleet which is larger than is economically ideal and has negative consequences for safety and the environment [13]. For example, under fishing derby management in Aitutakus in the Cook Islands, fishers damaged the reef by overloading their boats [1].

ITQs give individual fishers a right to a specified percent of the TAC each season, eliminating the various pressures of the race to fish. In the Alaskan Pacific halibut fishery, the ITQ system lengthened the fishing season from three 24-hour periods to 8 months. Mortality due to ghost fishing, the capture of fish in discarded fishing equipment, was immediately reduced by 80% [33].

Also, TAC is determined under uncertainty and in a manner subject to political pressure. If fishers are incentivized to overexploit, they can pressure managers to set TAC too high. ITQs can be bought and sold among fishers and, in some implementations, to non-fishers. The price of the quotas reflects the long-term value of the fishery, which gives them an incentive to preserve the resource for future years, so ITQs address the tragedy of the commons.

Importantly, ITQs do not solve the tragedy of the commons. Even under ITQs, an individual fisher who damages the fishery shares the cost with all quota holders. However, ITQs do address the tragedy of the commons, in that they provide some cost to the individual fisher, which is lacking in the absence of any stake in the future value of the fishery. Many studies show success for ITQs. In 2008, Costello et al. [19] found that fewer ITQ-managed fisheries were collapsed. ITQs are not perfect in preventing fishery collapse, but they tilt the odds against collapse.

In this thesis, we move a little beyond ITQs by providing a mechanism to sell back the quota, which reduces pressure on the population, especially if and when it declines. We run simulations from several initial overharvesting conditions to find management rules that could help correct this behavior, without assuming that anyone knows what the modeled optimal harvest is. In this sense, Chapter 3 is part of a small number of papers that we describe in the next few paragraphs that seek to decentralize decision making by simple rule.

In 1992, Townsend [54] proposed "bankable" ITQs that allow fishers who fish less than their entire quota in a given year to fish that quota in future years, with added interest equal to the growth rate of the fish stock, thus setting the annual quota in the hand of the

fishers for any given year.

In 2009, Arnason [5] even found that an ITQ system involving what he termed conservation ITQs eliminates the need for a central authority to set a TAC. In his system, fishers and conservation groups can trade quota, with quota held by conservation groups remaining unfished.

In 2013, Bishi et al [8] modeled allowing fishers to switch between two species by their own choice and found that it can create what they call a "self-regulating" fishery as fishers switch to the second species when one of the species becomes harder to find. Initially, they obtained this result for two species that do not interact, but they later found this result to hold even when the two species are in a predator-prey relationship.

Another goal of ours in modeling harvest behavior in Chapter 3 is to help make the management of fisheries and other common pool resources more understandable and therefore localizable. In 2003, Hilborn [35] proposed simple rules in fisheries management, in part so that the reasons for prediction could be better understood by the modelers. Elinor Ostrom studied successful common-pool resource management throughout her Nobel Laureate career ending in 2012. One of her findings [46] was that respect for the rules in resource management declines as managers become more removed from the resource extractors.

Chapter 2: The ratio-dependent predator-prey model with constant harvests

Consider a general predator-prey model:

$$\dot{x} = g(x) - yf(x, y) \tag{2.1}$$

$$\dot{y} = -h(y) + cyf(x, y),$$

where x is the population of the prey species, y is the population of the predator species, $g(x)$ describes the growth of the prey in the absence of predators, and $-h(x)$ describes the decay of the predators in the absence of prey. The term $yf(x, y)$ models predator-prey interaction, and the function $f(x, y)$ is known as the functional response. The unusual choice of notation, $yf(x, y)$, is based on the fact that several early functional responses, when defined in this way, were entirely prey-dependent - that is $f(x, y)$ was actually a function of x. In 1989, Arditi and Ginzburg proposed a ratio-dependent functional response with $f(x, y) = ax/(x + cy)$, so named because f is a function of x/y, and the associated predator-prey model:

$$\dot{x} = rx(1 - \frac{x}{M}) - \frac{axy}{x + cy} \tag{2.2}$$

$$\dot{y} = y\left(-d + \frac{bx}{x + cy}\right).$$

Simple calculation shows that model can be transformed to a scale-free form:

$$\dot{x} = x(1-x) - \frac{axy}{x+y} \tag{2.3}$$

$$\dot{y} = y\left(-d + \frac{bx}{x+y}\right),$$

where a,d, and b are positive constants.

Some empirical support has been found for this model as described in [2]. As we discuss in the next section, a rather extensive analysis of (2.3) was conducted in [57]. We study an extension of (2.3):

$$\dot{x} = x(1-x) - \frac{axy}{x+y} - h \tag{2.4}$$

$$\dot{y} = y\left(-d + \frac{bx}{x+y}\right) - k,$$

where the nonnegative constants h and k represent a constant harvest by human resource managers of each species. Because of the biological application and consistent with [57, 55, 56], we are only interested in solutions where $x, y \geq 0$, forming a region we will call P. We present these models in their scale-free form for analysis.

Analysis of (2.4) was proposed in [55]. However, this paper did not contain this analysis. To our knowledge, analysis of (2.4) is not present in the literature.

As we will discuss below, previous articles have demonstrated the existence of limit cycles for (2.3) and similar models. In theory, the existence of these limit cycles has consequences for resource managers, in that population changes might be neither the result of over- or under-fishing. The purpose of our study in this chapter is to explore the relevance of these limit cycles in practice.

The rest of this chapter is as follows: in Section 2.1, we discuss the analysis of some specific cases of our model in previous work. In Section 2.2, we give some analytical results

of our model, (2.4). In Section 2.3, we compare some of the properties of (2.4) with positive harvests to results from the special cases in the papers from Section 2.1. In Section 2.4, we present some basic numerical indications for (2.4). In Section 2.5, we describe the creation and results from a numerical limit cycle continuation procedure for (2.4) we created and implemented in MATLAB, beginning with some further analysis in support of that procedure. In Section 2.6, we demonstrate an analytical result that a predator harvest can prevent predator extinction under (2.4) for some parameter values and initial conditions. Finally, in Section 2.7, we apply (2.4) to the oyster and black drum populations in the public oyster areas of Louisiana.

2.1 Background

In [57], Xiao and Ruan analyzed the dynamics of (2.3) and determined all equilibria and their stability for the system. I will summarize their paper here since my work is closely related to this paper, and to [55] and [56]. Equation (2.3) is smooth in the interior of P and was extended to a Lipschitz system in P, by defining $\dot{x} = 0$ and $\dot{y} = 0$ when $(x, y) = (0, 0)$. Then (2.3) has 2 or 3 equilibria, depending on the parameters: $(0, 0), (1, 0)$, and (x^*, y^*) where

$$x^* = 1 - \frac{a(b-d)}{b}, y^* = \frac{b-d}{d}x^*,$$

when $(x^*, y^*) \in P$. For (1,0) and (x^*, y^*), the Jacobian is analyzed to determine the stability of the equilibria. The point (1,0) is always hyperbolic, except when $b = d$, for which $(1, 0)$ is a saddle-node point. The equilibrium (x^*, y^*) may also be nonhyperbolic. The equation for a surface of Hopf bifurcations corresponding to some (actually, most) of the parameters for which (x^*, y^*) is hyperbolic is also found. In this case, the Liapunov coefficient is used to determine that the Hopf bifurcations are supercritical. Of note, since a Hopf bifurcation surface exists, some parameter values must result in limit cycles since limit cycles always exist near Hopf bifurcations.

The Jacobian of (2.3) does not exist at the origin, so linear analysis is not possible for (2.3) in its original version. Stability at the origin was analyzed using the time transformation $d\tau = (x + y)dt$, which preserves stability in P. Under this transformation, $(0, 0)$ becomes a nonhyperbolic equilibrium, which was analyzed using a transformation to polar coordinates. Global dynamics are classified for some parameter values, using the boundedness of (2.3) and a previous result in [41] which rules out limit cycles when (x^*, y^*) is stable. The classification of all cases does not provide a formula distinguishing when the limit cycles created on the Hopf bifurcation surface disappear.

Phase portraits using XPP [26], a commonly used numerical software for differential equations, are also shown. Of note, the parameters used to plot a limit cycle ($a = 2, d = 0.5, b = 0.782$) give b to the thousandths position, whereas no other parameter was specified to greater than the tenth place and no parameter at all was specified in the other seven phase portraits to greater than the tenth place, which may suggest, as my numerical results given below also find for many Hopf points, that only a small range of parameter values can create a limit cycle.

In [55], a similar analysis was conducted for (2.4) with $k = 0$:

$$\dot{x} = x(1 - x) - \frac{axy}{x + y} - h \tag{2.5}$$

$$\dot{y} = y\left(-d + \frac{bx}{x + y}\right).$$

Here, Xiao and Jennings subtract a constant harvest from the prey species in (2.3), to model a prey species that has a constant human harvest in addition to its "natural" dynamics. As before, (2.5) is Lipschitz in P under the extension $\dot{x} = -h$ and $\dot{y} = 0$ when $(x, y) = (0, 0)$. The number of equilibria can vary from 0 to 4. Closed form formulas of the equilibria were calculated by setting both derivatives equal to zero. These formulas are given in [55] and not repeated here. Of note, when (2.5) has 1 or 2 equilibria, they occur on

the x-axis. When there are 3 or 4 equilibria, 2 are on the x-axis and the remaining equilibria are in the open first quadrant. In the case of 3 equilibria, the strictly positive equilibrium is a cusp of codimension 2, and the coordinate transformation to demonstrate this was given in the appendix of [55]. The case of a single equilibrium is also nonhyperbolic, and normal form analysis is also shown in the appendix for a single equilibrium. In this case, the equilibrium is a saddle-node bifurcation point if $b \neq d$, and a degenerate saddle-node of codimension 4 if $b = d$ and $2a - 5b \neq 0$. (No result is given for the case where $b = d$ and $2a - 5b = 0$.) Sketches of phase portraits for (2.5) with 1, 2, and 3 equilibria are given.

A bifurcation analysis is also conducted in [55]. The presence of two saddle-node bifurcation surfaces is clear from the analysis of the number of equilibria, and the formula for these surfaces is provided. A transformation of (2.5) to the normal form of a codimension 2 bifurcation, known as the Takens-Bogdanov bifurcation, is conducted. The transformation is known to be nonsingular by numerical computation for some parameter values, demonstrating the existence of a surface of Takens-Bogdanov bifurcations, as well as a surface of Hopf bifurcations and a surface of homoclinic bifurcations, since the latter bifurcations always exist near a Takens-Bogdanov bifurcation. As in [57], criticality (see Definition 2) of the Hopf bifurcations was analyzed using the Liapunov exponent. Hopf bifurcations of (2.5) may be either supercritical or subcritical, depending on the parameters. When $a < b$ at the saddle-node bifurcation, an orbit connecting the saddle-node bifurcation point and the saddle point on the x-axis is expected. Because of the number of free parameters, it is further expected that a surface exists near the saddle-node in the parameter space where a separatrix connects the two saddles. On this surface, a heteroclinic bifurcation would be expected. Explicit equations for the bifurcation surface are only calculated for the saddle-node bifurcations.

Finally, [56] conducts an analysis of the system with predator harvesting, i.e. (2.4) with $h = 0$:

$$\dot{x} = x(1 - x) - \frac{axy}{x + y} \tag{2.6}$$

$$\dot{y} = y\left(-d + \frac{bx}{x+y}\right) - k.$$

Again, (2.6) is Lipschitz with the proper extension, in this case $\dot{x} = 0$ and $\dot{y} = -k$ when $(x, y) = (0, 0)$. No equilibria exist on the axes. The number of equilibria was determined for all possible parameter values, and can be 0,1, or 2. In this case, setting both derivatives equal to zero and solving requires solving a cubic equation in a single variable. The number of equilibria in P was determined for all possible parameter values based on intermediate value theorem arguments. A closed form formula for the equilibrium was only found in the case where only a single equilibrium existed. In this case, the equilibrium is nonhyperbolic. Transformation to a normal form was conducted. When the trace of the Jacobian is zero (an explicit formula for this condition is provided in [56]), the equilibrium is a cusp. Otherwise, the equilibrium is saddle-node bifurcation point. In the case of 2 equilibria, the sign of the determinant of the Jacobian shows that one equilibrium is a node and the other is a saddle. The stability of the node was not determined. Limit cycles are not possible in the case of a single equilibrium, since it not possible for such a cycle to contain equilibria whose indices sum to 1. Thus, limit cycles are only possible in the case of two equilibria. Bifurcation analysis was also conducted. To simplify this analysis, attention was restricted to the case where $a = 1$, and formulas discussed earlier from the single-equilibrium case are translated to this case. The authors show by translation to normal form that when $a = 1$, the cusp is a Takens-Bogdanov bifurcation point. Again, analysis using the Liapunov exponent shows Hopf bifurcations may be either subcritical or supercritical, depending on the parameters.

2.2 Preliminary Analytical Results

2.2.1 Number and nature of equilibria

In this section we give some results on the number and nature of the equilibria of (2.4) under the assumption $h, k > 0$. Results for the number and type of equilibria when either harvest

is zero are given in the papers [57], [55], and [56], as discussed in the previous section.

We first note that there are no equilibria on the axes for (2.4) with positive harvests since plugging in $x = 0$ or $y = 0$ we see that $\dot{x} = -h \neq 0$ on the y-axis and $\dot{y} = -k \neq 0$ on the x-axis. With this result, the region where $h, k > 0$ is easily characterized, as shown in the following simple calculation:

Lemma 1. *Let a, b, d, x, y be positive numbers such that*

(i) $y < x(b/d - 1)$ and

(ii) $a < (x + y)(1 - x)/y$.

Then there exist unique positive values h and k such that (x, y) is an equilibrium for (2.4) with parameter values a, b, d, h, k. Conversely, if (x, y) is an equilibrium for (2.4) with parameter values a, b, d, h, k, then (i) and (ii) are satisfied.

Proof.

$$\begin{aligned} k = y(-d + bx/(x + y)) &> 0 \iff \\ -d + bx/(x + y) &> 0 \iff \\ -dx - dy + bx &> 0 \iff \\ dy &< x(b - d) \iff \\ y &< x(b/d - 1). \end{aligned}$$

$$\begin{aligned} h = x(1 - x) - axy/(x + y) &> 0 \iff \\ axy/(x + y) &< x(1 - x) \iff \\ ay &< (x + y)(1 - x) \iff \\ a &< (x + y)(1 - x)/y. \end{aligned}$$

□

Note that (i) implies $d < b$ and (ii) implies $x < 1$.

We now move to the number of equilibria. Simple calculation shows that when $k > 0$, the system $\dot{x} = 0, \dot{y} = 0$ is equivalent to:

$$Q(y) := bd^2y^4 + (-b^2d + ab^2d + bd^2 - 2abd^2 + ad^3 + 2bdk)y^3 +$$

$$(b^3h - 2b^2dh + bd^2h - b^2k + ab^2k + 2bdk - 4abdk + 3ad^2k + bk^2)y^2 + \tag{2.7}$$

$$(-2b^2hk + 2bdhk + bk^2 - 2abk^2 + 3adk^2)y + bhk^2 + ak^3 = 0$$

$$x = \frac{y(k + dy)}{-k + by - dy},$$

from which we can see there a unique equilibrium in P for each root of $Q(y)$ in the interval $[0, \frac{k}{b-d})$. Since $Q(y)$ is a quartic polynomial, we know that there are at most four equilibria for any choice of parameters.

We also note that $Q(0) = bhk^2 + ak^3 > 0$ and $Q(\frac{k}{b-d}) = \frac{b^3k^4}{(b-d)^4} > 0$, so, if there are no multiple roots (which would correspond to nonhyperbolic equilibria), there must be an even number of roots between 0 and $\frac{k}{b-d}$. We combine these results into the following Lemma.

Lemma 2. *For any choice of positive parameter values a, b, d, h, k, (2.4) has at most four equilibria. If all the equilibria are hyperbolic, then there are an even number of equilibria in P.*

In the case where all equilibria are hyperbolic, we can characterize the type of each equilibrium. To do so, we return to the analysis of (2.4). For now, we suppose that only $a, b, d > 0$ and $h \geq 0$ are given. We now let k vary along with x and y in our analysis. From the equation for $\dot{x}$, calculation shows that for any given $x \geq 0$, there is at most one y

(independent of k) where (2.4) could be at equilibrium, specifically

$$Y(x) := \frac{-x^3 + x^2 - hx}{x^2 - (1-a)x + h}.$$

We also have that any choice of x and y determines a unique k at equilibrium, specifically $k = y(-d+bx/(x+y))$. These two results combine to give us a function $K(x)$ that maps the x of each equilibrium (x, y) in P to the value of k where (x, y) is an equilibrium. Since K is the composition of two functions that are differentiable on their domain, K is differentiable. In fact, in the following Lemma, we see that for hyperbolic equilibria, $K'(x)$ is tied to the type of equilibrium:

Lemma 3. *Let (x, y) be a hyperbolic equilibrium of (2.4). Then (x, y) is a node if $K'(x) > 0$ and a saddle if $K'(x) < 0$.*

Proof. Let $f(x, y, k) = x(1-x) - \frac{axy}{x+y} - h, g(x, y, k) = y\left(-d + \frac{bx}{x+y}\right) - k$, J be the Jacobian of (2.4). Any branch of equilibria is given implicitly by $f(x, y, k) = g(x, y, k) = 0$. By standard multivariate calculus, $1/(K'(x))$ is the first coordinate of $-J^{-1}\begin{bmatrix} \frac{\partial f}{\partial k} \\ \frac{\partial g}{\partial k} \end{bmatrix}$, which, by simple calculation is $-\frac{\partial f}{\partial y}\frac{1}{\det(\mathrm{J})}$. From the trace-determinant plane, $\det(J) > 0$ at nodes, so the sign of $K'(x)$ is the same as the sign of $-\frac{\partial f}{\partial y}$, which is $\frac{ax^2}{(x+y)^2}$, which is positive in P. Since from the trace-determinant plane, $\det(J) < 0$ at saddles, we similarly have $K'(x)$ is negative at saddles. □

From its component functions, $K(x)$ is a rational function of x. In the following result, we show that, on the domain appropriate to our problem, K does not have asymptotic behavior.

Lemma 4. *Restrict the domain of $K(x)$ to those equilibria where $(x, Y(x))$ is in P and $K(x) \geq 0$. Then the domain of $K(x)$ is bounded, and K is 0 on the boundary of the domain.*

Proof. We know the domain is bounded, since x is non-negative and we saw above that $x < 1$. As before, there are no equilibria when $x = 0$ since $\dot{x} = -h \neq 0$ in that case. Factoring out $-x$ from $Y(x)$, we have

$$Y(x) = -x\frac{x^2 - x + h}{x^2 - (1-a)x + h}.$$

Let $N(x) = x^2 - x + h, D(x) = x^2 - (1-a)x + h$. For $Y(x) \geq 0$, we must have $N(x)/D(x) \leq 0$. The only difference between the polynomials $N(x)$ and $D(x)$ is the coefficient on x. In fact, $N(x) = D(x) - ax < D(x)$, so $N(x)/D(x)$ is non-positive precisely when $N(x) \leq 0 < D(x)$, and the domain is contained in the region where this is true.

We now consider the sign of K on the region where $Y(x)$ is positive. Since $K(x) = Y(x)(-d + bx/(x + Y(x)))$, when $Y(x) > 0$, the sign of $K(x)$ is determined by the sign of $-d + bx/(x + Y(x))$, which, by simple calculation is $\frac{b}{ax}(x^2 - (1 - (1 - d/b)a)x + h)$, and eliminating known positive quantities again, this is determined by the sign of $S(x) := (x^2 - (1 - (1 - d/b)a)x + h)$, which again differs from $N(x)$ only in its coefficient of x. Since $S(x) - D(x) = -\frac{ad}{b}x$, we know $S(x) < D(x)$. Specifically, $S(x)$ is negative when $D(x) = 0$, so the domain of K does not approach the points where $D(x) = 0$. Now $N(x) - S(x) = a(1 - d/b)x > 0$, using the inequality we saw above that $d/b < 1$ at an equilibrium in P, and the domain of K is the set of points where $N(x) \leq 0 \leq S(x)$. Finally $K(x) = 0$ when $N(x) = 0$, since $N(x) = 0$ implies $Y(x) = 0$. The function $K(x) = 0$ when $S(x) = 0$ since $K(x) = \frac{b}{ax}S(x)$. □

The previous result allows a better characterization of the equilibria when they are hyperbolic.

Theorem 1. *Let $a, b, d, h, k > 0$ be parameter values and $\{(x_1, y_1), (x_2, y_2), ...(x_n, y_n)\}$ be the equilibria for* (2.4) *for those parameter values, arranged in order of increasing x-values. (As we have seen above, these x-values must be distinct.) Then if all equilibria are hyperbolic,*

(x_m, y_m) is a node for odd m and (x_m, y_m) is a saddle for even m.

Proof. Consider (x_1, y_1). Since (x_1, y_1) is an equilibrium in P, x_1 is in the domain of K and $K(x_1) = k > 0$. The domain of K may be disconnected, but x_1 is on some connected portion of the domain, which has a lower bound $\omega < k$ where $K(\omega) = 0$. Since $K(x)$ does not obtain the value k until x_1, by continuity $K(x)$ must thus be increasing when it reaches $x = x_1$. (We have assumed hyperbolicity, so x_1 may not be an extremum of K.) Thus, by Lemma 3, (x_1, y_1) is a node.

Also, since K is increasing at x_1, $K(x) > k$ for x just above x_1, and so at the next equilibrium x-value, x_2, $K(x)$ must be decreasing, and (x_2, y_2) must be a saddle.

In this way, we have alternating stability type on each connected component of the domain. To see alternating stability type overall, we note that since $K(x)$ is 0 on both endpoints of each connected component, there must be an even number of crossings of the value k on each component. □

Note: We have shown this result in the case of positive harvest. A review of the equilibrium results from [55] and [56] shows that this result extends to the case where one harvest is zero. From [57], the origin is always nonhyperbolic when both harvests are zero and this result would technically extend vacuously to that case as well.

2.2.2 Bifurcation results

In this section, we will provide some results related to the bifurcations of (2.4) as the predator harvest, k, varies. We begin by providing an equation for the bifurcation surfaces of (2.4). Certain common factors recur in the formulas for bifurcation surfaces. If we let:

$$z = ay^2$$

$$v = bx^2 \tag{2.8}$$

$$w = d(x + y)^2$$

$$j = (2x - 1)(x + y)^2,$$

then by straightforward calculations using Mathematica, under (2.8), the eigenvalues of the Jacobian of our system are:

$$\frac{v - z - w - j \pm \sqrt{(v - z - w - j)^2 + 4(jv - wz - jw)}}{2(x + y)^2}.$$

We have not converted the denominator to the new coordinates because for the bifurcation analysis below it is irrelevant, except to note that it is always positive unless $x = -y$, which is never true in the interior of P or on the boundary except at (0,0). Let $f_1 = v - z - w - j$, $f_2 = jv - wz - jw$. We analyze the numerator, $f_1 \pm \sqrt{{f_1}^2 + 4f_2}$. We have:

- At a saddle-node bifurcation, $f_2 = 0$, since $f_1 \pm \sqrt{f_1^2 + 4f_2} = 0 \iff f_2 = 0$.
- At a Hopf bifurcation, $f_1 = 0$ and $f_2 < 0$ since these conditions establish that $f_1 \pm \sqrt{f_1^2 + 4f_2}$ will be purely imaginary.

Furthermore, a double-zero eigenvalue occurs when $f_1 = 0$ and $f_2 = 0$. The Takens-Bogdanov bifurcation is the generic bifurcation that occurs when the Jacobian of a system has a double-zero eigenvalue. We use generic in the sense of [42], p. 78, that a property is generic "if systems from the intersection of a countable number of open and dense subsets of D possess this property," where D is a space of dynamical systems. Heuristically, this means that a Takens-Bogdanov bifurcation usually occurs at an equilibrium whose Jacobian has a double-zero eigenvalue. There are, however, certain "nongeneric" conditions, known as degenerate cases, under which a double-zero does not result in a Takens-Bogdanov bifurcation. We will look at the degenerate cases for (2.4) in Section 2.2.3.

Furthermore, it is possible to analyze (2.4) in terms of its bifurcations, and then "force" the system into equilibrium using the harvests h and k which do not occur in the Jacobian. For any choice of a, b, d, x, and y, there is a unique (but not necessarily positive) choice of

h and k that brings the system to equilibrium:

$$h = x(1-x) - \frac{axy}{x+y}$$

$$k = y(-d + \frac{bx}{x+y}).$$

In this way, the constant harvest allows us to implicitly identify the bifurcation surfaces of (2.4). It is not necessary to first find the equilibria and then find the Jacobian at the equilibria. The nature of the constant harvests is such that we can analyze the Jacobian for bifurcation criteria and then adjust the harvest to find the equilibria.

Interestingly, this also shows that any positive value of z, v, and w, and any real j corresponds to some equilibrium in P with positive parameters under (2.8). To show this, we first note that a straightforward calculation shows that when $j \neq 0$, (2.8) is solved by

$$a = \frac{z}{\left(\sqrt{\frac{j}{2x-1}} - x\right)^2}$$

$$b = \frac{v}{x^2} \tag{2.9}$$

$$d = \frac{w(2x-1)}{j}$$

$$y = \sqrt{\frac{j}{2x-1}} - x.$$

The solution leaves us free choice of x since the space formed by z, v, w, and j has one less dimension than the space formed by a, b, d, x, and y. Further calculation using this solution

shows that (i) in Lemma 1 is equivalent to

$$\frac{v^2 j}{x^2 w^2 (2x-1)} > 1$$

and that (ii) is equivalent to

$$z < \left(\sqrt{\frac{j}{2x-1}} - x \right) \sqrt{\frac{j}{2x-1}} (1-x).$$

Note that for any $z, v, w > 0$ and $j \in \mathbb{R}$, some x in the neighborhood of $1/2$ will satisfy (i) and (ii).

When $j = 0$, (2.8) is solved by

$$x = \frac{1}{2}$$

$$b = 4v \tag{2.10}$$

$$a = \frac{z}{y^2}$$

$$d = \frac{w}{(y + \frac{1}{2})^2}.$$

Now straightforward calculation shows that (i) is equivalent to

$$y < \frac{2v(y + \frac{1}{2})^2}{w} - \frac{1}{2}$$

and (ii) is equivalent to

$$z < \frac{1}{2} y \left(y + \frac{1}{2} \right).$$

Note that again some solution to (i) and (ii) exists for any $z, v, w > 0$. In this case, choosing y high enough will satisfy both inequalities.

Thus, (2.8) makes testing the bifurcation conditions simple. The nature of our transformation is such that this does not easily translate to a solution for x and y in terms of the parameters, but it does easily translate into a solution for one or two parameters in terms of x and y and the other parameters.

2.2.3 Conditions for Takens-Bogdanov Bifurcations

In the previous section, we noted that Takens-Bogdanov bifurcations typically exist at double zero eigenvalues. In this section, we will give precise conditions, in terms of the parameters, for Takens-Bogdanov bifurcations varying the two parameters b and k, including formulas for the degenerate cases.

In this section we will use the notation $f(x,y) := \dot{x} = x(1-x) - \frac{axy}{x+y} - h, g(x,y) := \dot{y} = y\left(-d + \frac{bx}{x+y}\right) - k$, and let J refer to the Jacobian of (2.4). We will use subscript notation for partial derivatives, for example $f_y := \frac{\partial f}{\partial y}$. We will be interested only in those points in the interior of our phase space and parameter space, because we wish to find points where all bifurcation behavior is in the region of biological interest, so we will assume all variables and parameters are strictly positive.

For a Takens-Bogdanov bifurcation, we need $f = g = f_1 = f_2 = 0$, where f_1 and f_2 are the functions defined in the previous section. A long but straightforward calculation shows that when $f = g = 0$, the equations $f_1 = f_2 = 0$ are equivalent to:

$$q = \frac{x^3(2x-1)}{(x+y)(x^2(2x-1) + (-h+x^2)y)}$$

$$b = \frac{-x^3 + 2x^4 - hxy - x^2y + 3x^3y - hy^2 + x^2y^2}{x(x^2 - qx^2 - 2qxy - qy^2)} \tag{2.11}$$

$$d = qb$$

where $q := d/b$ is introduced for notational convenience. We will see q again in Section 2.5.1. Note that for any x, y, h, (2.11) gives a unique, if defined q, a, b, k, and d. We also note that numerical calculation shows that there exist solutions where all parameters are positive (for example $x = 0.3, y = 1, h = 0.1, a \approx 0.477, b \approx 0.926, d \approx 0.167, k \approx 0.046$).

We now seek to rule out the degenerate cases. From Theorem 8.4 in [42], we avoid the degenerate cases if:

$$J \neq 0 \tag{2.12}$$

$$f_{xx} + g_{xy} \neq 0 \tag{2.13}$$

$$g_{xx} \neq 0 \tag{2.14}$$

and the map

$$(x, y, b, k) \mapsto (f, g, \mathrm{tr(J)}, \det(\mathrm{J})) \tag{2.15}$$

is nonsingular, where *tr* and *det* refer to the trace and determinant.

First note that since $f_y = -\frac{ax^2}{(x+y)^2} \neq 0$, (2.12) is always true in the interior of P. We also have $g_{xx} = -\frac{2by^2}{(x+y)^3} \neq 0$ and (2.14) is always true in the interior of P.

To check (2.4), we compute $f_{xx} + g_{xy} = -2 + \frac{2ay(y-x)}{(x+y)^3}$, which is nonzero precisely when $ay(y-x) \neq (x+y)^3$.

Finally, we need to consider the map in (2.15). We need to analyze the Jacobian of that map:

$$\begin{bmatrix} 1 - 2x - \frac{ay^2}{(x+y)^2} & -\frac{ax^2}{(x+y)^2} & 0 & 0 \\ \frac{by^2}{(x+y)^2} & -d + \frac{by^2}{(x+y)^2} & \frac{xy}{x+y} & -1 \\ -\frac{2(x^3-bxy+3x^2y-ay^2+3xy^2+y^3)}{(x+y)^3} & -\frac{2x(bx+ay)}{(x+y)^3} & \frac{x^2}{(x+y)^2} & 0 \\ \frac{2(-bx^3+dx^3+bxy-3bx^2y+3dx^2y-ady^2+3dxy^2+dy^3)}{(x+y)^3} & \frac{2x(bx(-1+2x)+ady)}{(x+y)^3} & \frac{(1-2x)x^2}{(x+y)^2} & 0 \end{bmatrix},$$

which has determinant:

$$\frac{2ax^3(-bx^3+dx^3+bxy-3bx^2y+3dx^2y-ady^2+3dxy^2+dy^3)}{(x+y)^6}.$$

Since the terms we factored out are known to be nonzero, this is equivalent to the condition $bx^3-dx^3-bxy+3bx^2y-3dx^2y+ady^2-3dxy^2-dy^3\neq 0$.

We combine these results into the following theorem:

Theorem 2. *Let (x,y) with $x,y>0$ be an equilibrium of (2.4) with parameter values $a,b,d,h,k>0$, and define $q:=d/b$. Then (x,y) is a Takens-Bogdanov bifurcation point with bifurcation parameters b and k if all of the following conditions hold:*

$$q=\frac{x^3(2x-1)}{(x+y)(x^2(2x-1)+(-h+x^2)y)}$$

$$b=\frac{-x^3+2x^4-hxy-x^2y+3x^3y-hy^2+x^2y^2}{x(x^2-qx^2-2qxy-qy^2)}$$

$$ay(y-x)\neq(x+y)^3$$

$$bx^3-dx^3-bxy+3bx^2y-3dx^2y+ady^2-3dxy^2-dy^3\neq 0$$

Note that numerical calculation shows that the nondegeneracy conditions at $x=0.3, y=1, h=0.1, a\approx 0.477, b\approx 0.926, d\approx 0.167, k\approx 0.046$ become $0.334\neq 2.197$ and $-0.291\neq 0$, which are both satisfied, so nondegerate Takens-Bogdanov bifurcations occur for (2.4). There is always a curve of Hopf bifurcations and a curve of homoclinic bifurcations near a Takens-Bogdanov bifurcation. Those two bifurcations will be important in our limit cycle continuation in Section 2.5.

Table 2.1: Comparison of results for model with a positive harvest of both species to special case results without one or both of the harvests.

	$h = k = 0$	$h = 0, k > 0$	$h > 0, k = 0$	$h, k > 0$
reference	[57]	[56]	[55]	this dissertation
simultaneous extinction	yes	no	no	yes
equilibrium at origin	yes	no	no	no
equilibrium on x-axis	2	0-2	0	0
equilibrium in interior	0-1	0-2	0-2	0-4
limit cycle stability	stable	stable or unstable	stable or unstable	stable or unstable
non-extinct global attractor	possible	not possible	not possible	not possible
Is x-axis invariant?	yes	yes	no	no
Is y-axis invariant?	yes	no	yes	no
Is P invariant?	yes	no	no	no
Takens-Bogdanov bifurcation	no	yes	yes	yes
Notable parameter choices	$a = 2, d = 0.5$ $b = 0.782$ to show limit cycle	$a = 1$ to simplify Takens-Bogdanov analysis	none	$a = 0.1, h = 0.2$ $d = 0.3$ and $a = 2, h = 0$ $d = 0.5$ for preliminary numerical indications

2.3 Comparison to models with $h = 0$ or $k = 0$

In this section, we compare the properties of the model (2.4) with the results from the papers [55], [56], and [57], which considered the special cases of the model where $h = 0$ or $k = 0$ or both, respectively. A nonhyperbolic equilibrium at the origin exists if and only if $h = k = 0$. The origin is not an equilibrium if either h or k is positive. Excepting the origin, equilibria do not exist on the y-axis in any case. Another equilibrium on the boundary of P exists when $h = k = 0$, on the x-axis at (1,0). Between 0 and 2 equilibria exist on the x-axis when $h > 0$ and $k = 0$. No equilibria exist on either axis when $k > 0$. The number of equilibria in the interior can be 0 or 1 when $h = k = 0$. There can anywhere from 0 to 2 equilibria in the interior of P when exactly one of the harvests is positive, and there can be 0 to 4 equilibria in the interior of P when both harvests are positive. Limit cycles may exist in all four cases, but when $h = k = 0$, it is known that the limit cycle must be unique and stable. Unstable limit cycles exist for some parameter values when either harvest is positive. We are not aware of any analytical result for uniqueness of the limit cycle when either harvest is positive. When both harvests are 0, P is an invariant set and it is possible for there to be a global attractor other than extinction, but when either harvest is positive, there is some portion of P where forward orbits leave P and extinction is predicted in forward time. Takens-Bogdanov bifurcations exist when either harvest is positive. They do not exist when h and k are 0. When $h = k = 0$, simultaneous extinction is possible: a forward orbit may approach the origin. When exactly one of the harvests is positive, simultaneous extinction is impossible. However, when both harvests are positive, simultaneous extinction again becomes possible, since the first order approximation of the slope of trajectory at the origin is the positive value k/h. The y-axis is invariant if and only if $h = 0$. The x-axis is invariant if and only if $k = 0$.

As noted in Section 2.1, the rather precise parameter choices $a = 2, d = 0.5, b = 0.782$ were used in [57] to plot a limit cycle and the simplification $a = 1$ was used to reduce (2.6) to normal form in [56]. We will use the limit cycle choice from [57] ($a = 2, h = 0, d = 0.5$) in our preliminary numerics in the next section as well as the completely arbitrary choice

$a = 0.1, h = 0.2, d = 0.3$.

2.4 Preliminary Numerical Indications

In this section, we create bifurcation diagrams for some parameter values of (2.4). As mentioned in Section 2.2.1, solving for the equilibria of (2.4) involves solving a quartic equation, so (2.4) can have up to 4 solutions. In fact, there are typically 0, 2, or 4 solutions, depending on the parameters. We created phase portraits in pplane [50], a package for creating phase portraits in MATLAB. A detailed description of pplane and its methods is available in [6]. Some phase portraits are shown in Figure 2.1.

We now turn to bifurcation analysis. Setting (by completely arbitrary choice) $a = 0.1$, $h = 0.2$, $d = 0.3$, we get the bifurcation diagrams shown in Figure 2.2 using AUTO [24].

The qualitative changes that occur as b increases correspond to passing through Takens-Bogdanov points which create Hopf bifurcations. The Hopf and saddle-node bifurcations (on the same branch) are always extremely close to each other (in k).

We have also conducted further numerical experiments, allowing d to vary. We found that the picture is qualitatively similar to that described above as long as $d > 0.2$ (keeping our arbitrary choice of $a = 0.1$ and $h = 0.2$). As d decreases, the b-value of the Takens-Bogdanov point increases. At $d = 0.2$, one Takens-Bogdanov point occurs when $b = \infty$ (i.e., it no longer exists), the b-value for the second Takens-Bogdanov point reaches infinity when d is slightly less than 0.2.

Letting k_{Hopf} and k_{sn} denote the k-values at the Hopf and saddle-node bifurcations, k_{Hopf}/k_{sn} is 1 at the Takens-Bogdanov point, decreases as b increases, remaining between 0.99 and 1, and then k_{Hopf}/k_{sn} increases as b goes to infinity, or at least several orders of magnitude beyond the Takens-Bogdanov point or any other observed interesting behavior, whenever $a = 0.1$ and $h = 0.2$. In other words, the Hopf and saddle-node bifurcations are quite close to each other on each branch in this case, and the limit cycles formed at the Hopf points form away from the saddle-node and disappear quickly in a homoclinic bifurcation.

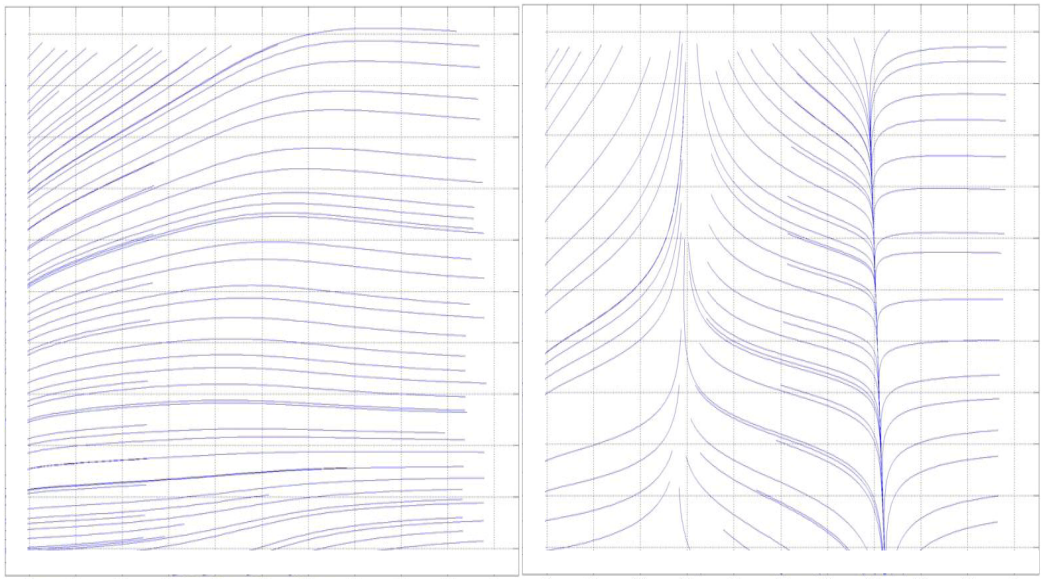

(a)

(b)

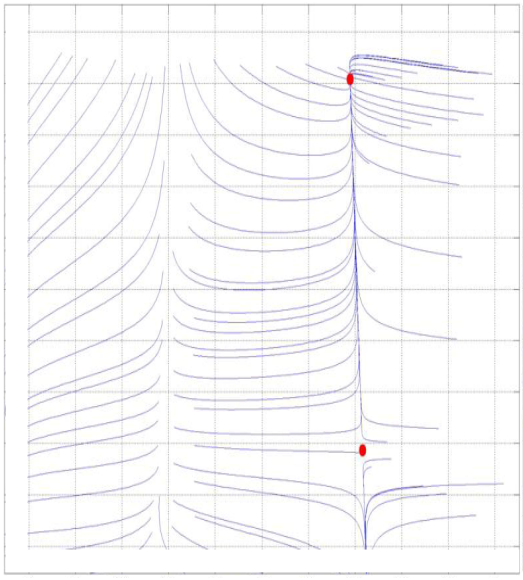

(c)

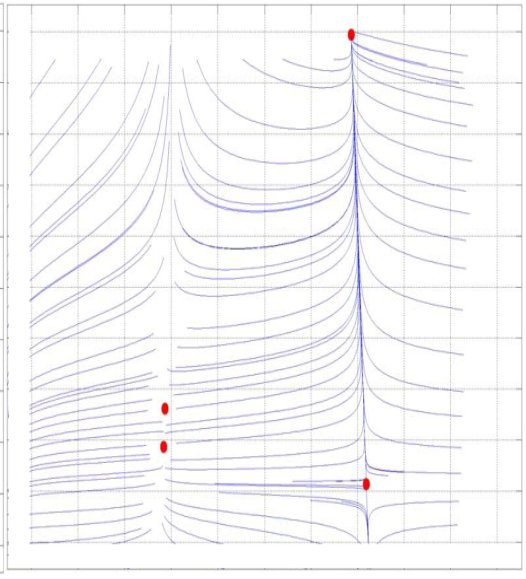

(d)

Figure 2.1: Phase portraits for (2.4): the ratio-dependent predator-prey system with constant harvests of both species from pplane. Only forward orbits are shown and all equilibria are marked. In all portraits, we use the parameter choices $a = 0.1$, $d = 0.3$, $b = 0.4$. We use $h = 0.2$, except in (a) where $h = 0.3$ to show a portrait where the prey harvest is too large to support any prey population. The parameter k decreases from 6E-3 in (b) to 3E-3 in (c) to 2E-3 in (d).

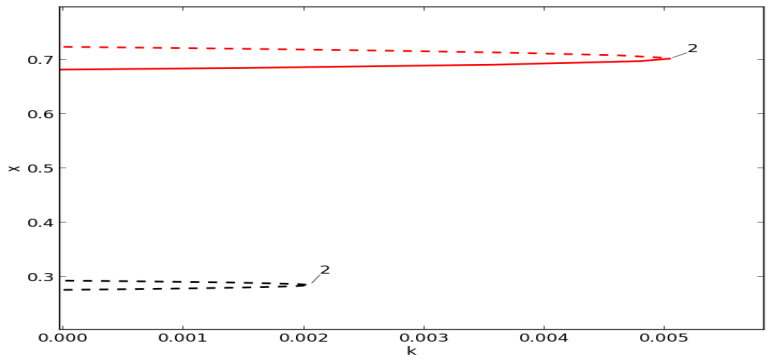

(a) $b = 0.4$

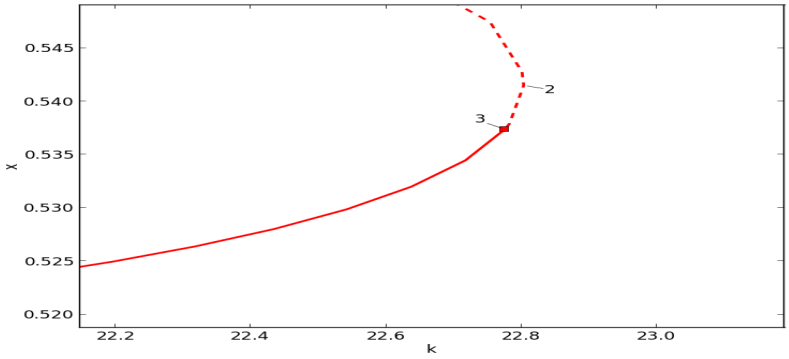

(b) $b = 50$

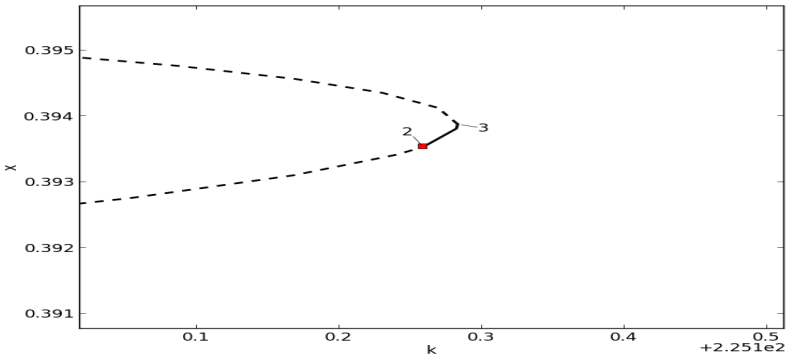

(c) $b = 600$

Figure 2.2: Bifurcation diagrams for (2.4) created in AUTO. In all diagrams, we use the parameter choices $a = 0.1$, $h = 0.2$, $d = 0.3$. The top diagram shows the general outline. When $b > 18.7$ a change in stability occurs on the top branch that is only visible on extreme close-up. When $b > 187$, a similar phenomenon happens on the bottom branch. These values of b correspond to passing through Takens-Bogdanov bifurcations.

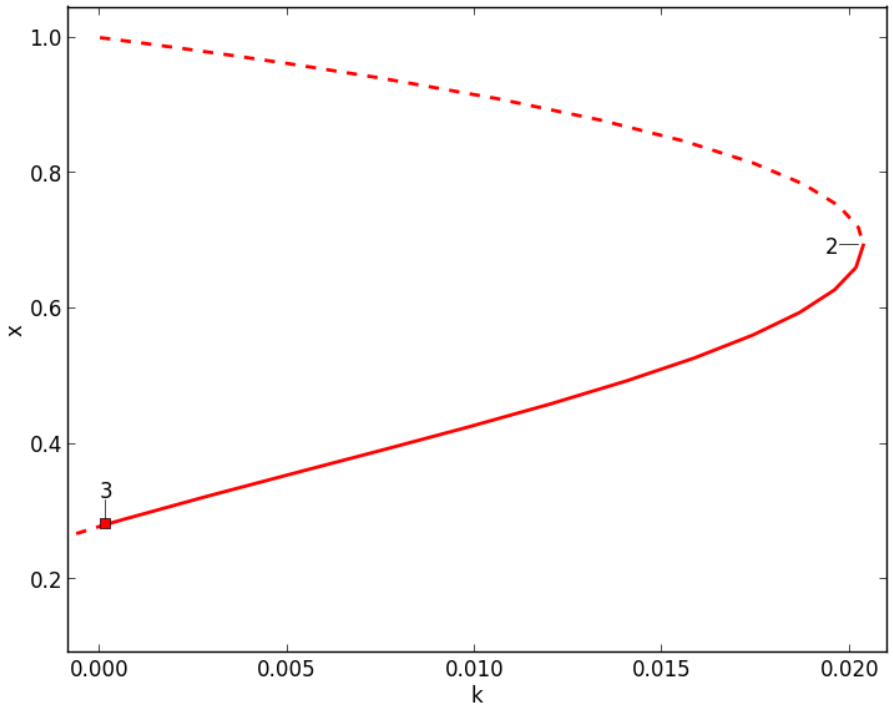

Figure 2.3: A bifurcation diagram created in AUTO for the parameter values $a = 2$, $h = 0$, $d = 0.5$, $b = 0.782$.

These behaviors are seen for many Hopf points of the model, which inspired the limit cycle continuation discussed below in the next section.

We now consider the parameter choices $a = 2$, $h = 0$, $d = 0.5$. The parameters are chosen because they are the values that led to the limit cycle shown in Figure 4.7 of [57]. A bifurcation diagram using the b-value from that figure, $b = 0.782$, is shown in our Figure 2.3. Note that now the Hopf bifurcation is no longer close to a saddle-node, but it is close to the boundary of our region of interest at $k = 0$. Some more bifurcation diagrams for $a = 2$, $h = 0$, $d = 0.5$ are shown in Figure 2.4. Here we see a different pattern than with our previous choice of a, h, and d. First, the diagram consists of one connected curve rather than two. Perhaps more interestingly, the changes as k increases are different. As before, a Hopf point begins to be seen as k increases. However, this change does not represent a Takens-Bogdanov bifurcation. The change represents a Hopf that enters the parameter

region of interest by passing through $k = 0$. In the middle diagram (where $b = 1$), we see a Hopf bifurcation that is neither near a saddle-node nor the boundary where $k = 0$. As b increases further, we pass through a Takens-Bogdanov, after which the Hopf is no longer seen. As seen in the middle diagram, we have a parameter choice showing a Hopf can be seen away from the saddle point, which, as we discussed above, wasn't observed for any b or d when we fixed $a = 0.1$ and $h = 0.2$.

2.5 Limit cycle continuation

In this section, we describe a limit cycle procedure created in MATLAB. All the MATLAB files are included in the supporting online materials available at `mason.gmu.edu/~mcrone`. We begin in Section 2.5.1 with further analytical results that were needed to support our implementation. Section 2.5.2 describes the algorithm employed in MATLAB. Section 2.5.3 describes how we confirmed the accuracy of the results on a subset of points. Finally, Section 2.5.4 gives the numerical results that we obtained.

2.5.1 Analytic results for limit cycle continuation

We begin with some further analysis of the Hopf surface. Since (2.4) has two variables and five parameters, and a Hopf bifurcation of (2.4) has three equality constraints $\dot{x} = 0, \dot{y} = 0$, and $f_1 = 0$, this is a four-dimensional surface. We want to create a finite grid of mesh points to cover the region, but the region is unbounded. However, some of the dimensions are bounded, as we found in Lemma 1:

- From the equation $\dot{x} = x(1-x) - \frac{axy}{x+y} - h$: $x < 1$ and $h < x(1-x)$.
- From the equation $\dot{y} = y\left(-d + \frac{bx}{x+y}\right) - k$: $d < b$.
- We set $q = d/b$. We treat q as a parameter: $\dot{y} = y\left(-qb + \frac{bx}{x+y}\right) - k$. This "cheat" creates a third bounded dimension.

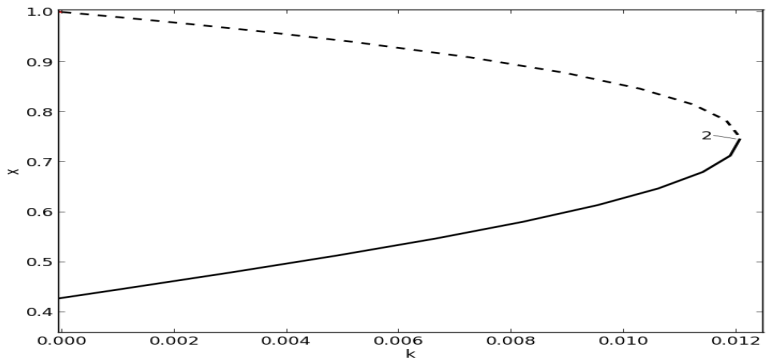

(a) $b = 0.7$

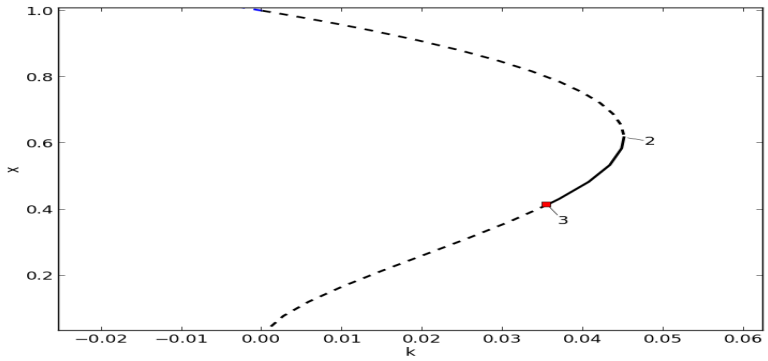

(b) $b = 1$

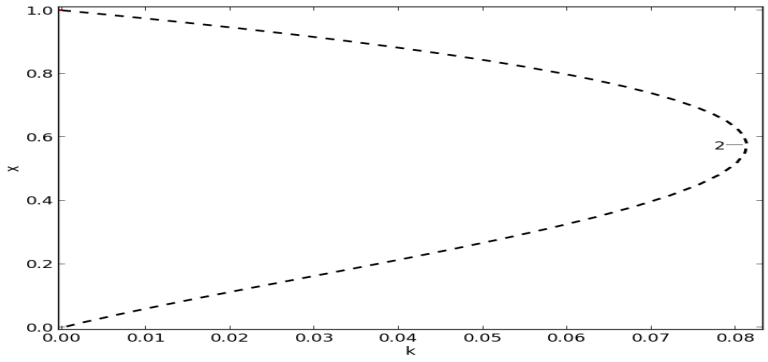

(c) $b = 1.3$

Figure 2.4: Bifurcation diagrams for (2.4) created in AUTO. In all diagrams, we use the parameter choices $a = 2$, $h = 0$, $d = 0.5$. When $b > 0.781$, a change in stability occurs along the curve. This value corresponds to where the Hopf bifurcation crosses the value $k = 0$. When $b > 1.203$, there is no longer a change in stability on the curve, and there is now no stable portion of the curve. The value of $b \approx 1.203$ corresponds to a Takens-Bogdanov bifurcation.

Note that if x, h, q, and y are given, the three equality constraints become linear in the remaining parameters. Calculation shows that the equality constraints are solved by:

$$a = \frac{(x(1-x)-h)(x+y)}{xy}$$

$$b = \frac{-x^3 + 2x^4 - hxy - x^2y + 3x^3y - hy^2 + x^2y^2}{x(x^2 - qx^2 - 2qxy - qy^2)} \tag{2.16}$$

$$k = -qby + \frac{bxy}{x+y}.$$

By further calculation using Mathematica, we can find a point on our Hopf surface iff q is greater than exactly one of the following functions:

$\frac{x}{x+y}$	(where $k = 0$)
$\left(\frac{x}{x+y}\right)^2$	(where $b = \infty$)
$\frac{x^3(2x-1)}{(x+y)(x^2(2x-1)+(-h+x^2)y)}$	(The Takens-Bogdanov surface: $f_1 = f_2 = 0$).

Thus, we have a one-to-one correspondence between points in (x, h, q, y)-space that satisfy this property and the Hopf surface of (2.4). Which inequalities form the boundary of the slice of the Hopf surface depends on x and h. There are three non-null cases depending on whether $x > 1/2$, $\sqrt{h} < x < 1/2$, or $x < \sqrt{h}$. Graphs of two-dimensional slices of this region are shown in Figure 2.5. Since all of the formulas approach the x-axis as $y \to \infty$, the Hopf surface becomes infinitely thin in y as $y \to \infty$, and for any finite grid size, there will be a finite number of points on the grid in x, h, q, y-space. We used such a grid to track the limit cycles formed at each grid point. The details of our search are given in the next section.

Our continuation described below in Section 2.5.2 is based on Poincaré sections and the Poincaré map, a theory which is described in detail in [48], a method based on the map from the points on a line segment. We summarize here. In a planar system such as (2.4), the Poincaré map is a function in one dimension. Consider a point (x_1, y_1) along some line

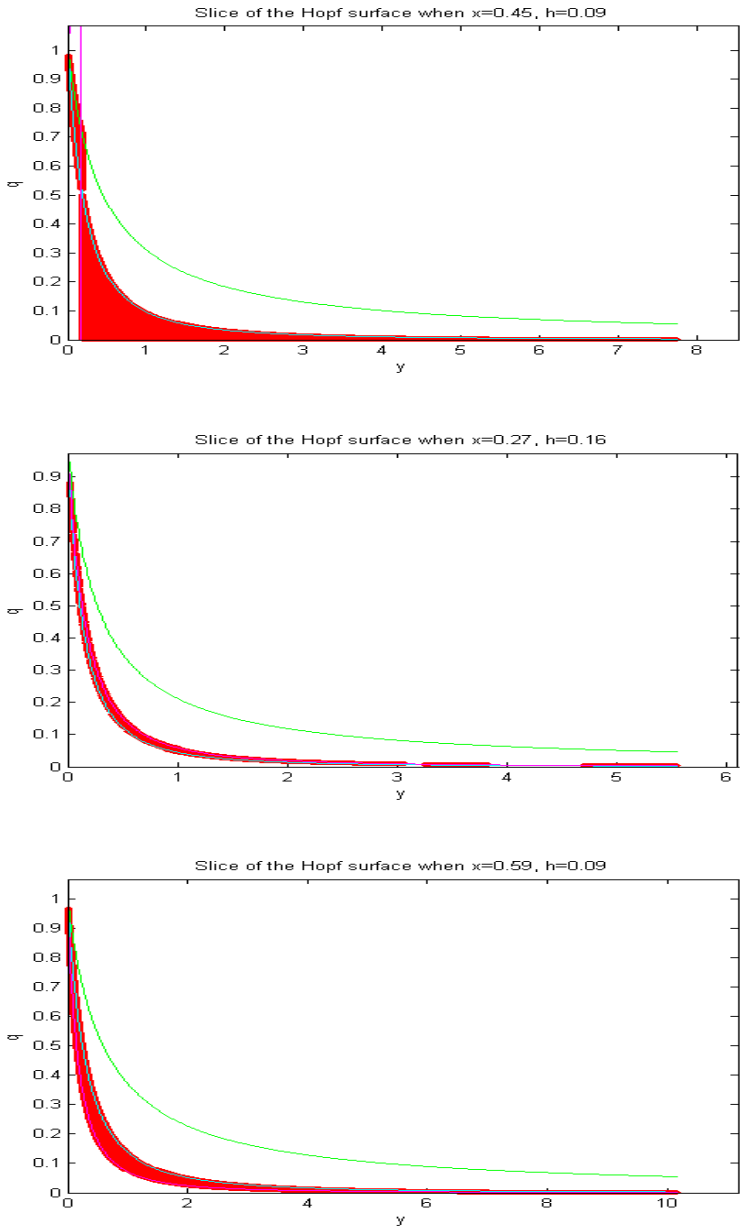

Figure 2.5: Slices of the Hopf surface representing three cases for the bounding functions of the slice.

segment in phase space, and suppose that the forward flow from (x_1, y_1) under (2.4) returns to the line segment at (x_2, y_2). Then the Poincaré map (for (2.4) and that line segment) maps (x_1, y_1) to (x_2, y_2). It is typical to identify the points on line segment with a single number (for example, their x-coordinate or their distance from some point) and treat this map as a function of a single variable. A fixed point of this map means that a limit cycle crosses the line segment at this point. For an analytic system, the Poincaré map is analytic, and the lowest-order nonzero coefficient in the Taylor expansion of the Poincaré map is of particular importance:

Definition 1. *The lowest order coefficient in the Taylor expansion of the Poincaré map is called the Liapunov number.*

Generically, the Liapunov number at a limit cycle is a coefficient on an odd power. In this case, a negative Liapunov number means the limit cycle is stable, and a positive Liapunov number means the limit cycle is unstable. A general formula for the Liapunov number at a Hopf bifurcation is given in [3]. Specifically, this source provides the third derivative of the Poincaré map using a Poincaré section that extends horizontally to the right of the equilibrium. The formula, in the notation of [3], is:

$$-\frac{\pi}{4b\beta^3}\{[ac(a_{11}^2 + a_{11}b_{02} + a_{02}b_{11}) + ab(b_{11}^2 + a_{20}b_{11} + a_{11}b_{20}) +$$

$$c^2(a_{11}a_{02} + 2a_{02}b_{02}) - 2ac(b_{02}^2 - a_{20}a_{02}) - 2ab(a_{20}^2 - b_{20}b_{02}) -$$

$$b^2(2a_{20}b_{20} + b_{11}b_{20}) + (bc - 2a^2)(b_{11}b_{02} - a_{11}a_{20})] \tag{2.17}$$

$$-(a^2 + bc)[3(cb_{03} - ba_{30}) + 2a(a_{21} + b_{12}) + (ca_{12} - bb_{21})]\}$$

where $\begin{bmatrix} a & b \\ c & d \end{bmatrix}$ is the Jacobian at the Hopf point, β^2 is the determinant of the Jacobian, a_{mn} is the coefficient of $x^m y^n$ in the Taylor expansion of $\dot{x}$ at the Hopf point, and b_{mn} is

the coefficient of $x^m y^n$ for $\dot{y}$. We determine the direction in which the limit cycle opens from the derivative of the trace of the Jacobian with respect to k as shown below:

Theorem 3. *Let k_0 be the k-value at a Hopf bifurcation and let L be the Liapunov number at the Hopf bifurcation as defined in the previous paragraph. As k varies, there will be a branch of equilibria $(x(k), y(k))$ near $k = k_0$. Let $T(k)$ be the trace of the Jacobian of the equilibrium along that branch as a function of the parameter k. Let $E = -sign(LT'(k_0))$. Then, provided E is nonzero, E gives the opening direction of the limit cycles at k_0. That is, the limit cycles form to the left of k_0 when $E = -1$ and to the right of k_0 when $E = 1$.*

Proof. From [48], the Hopf bifurcation is non-degenerate when $L \neq 0$. Thus, by our formula for E, the Hopf is non-degenerate since by hypothesis $E \neq 0$.

The trace is zero and the eigenvalues are purely imaginary at a Hopf point of a planar system. Now consider the eigenvalues. Let $D(k)$ be the determinant of the Jacobian of the continuation. From basic linear algebra, the eigenvalues of the Jacobian are $(T(k) \pm \sqrt{T(k)^2 - 4D(k)})/2$. These values are purely imaginary, so $T(k_0)^2 - 4D(k_0) < 0$. By continuity, $\sqrt{T(k)^2 - 4D(k)}$ is purely imaginary in some neighborhood of the Hopf and the real part of the eigenvalues (which gives the stability of the equilibrium) is $T(k)/2$. Thus, in some neighborhood of $k_0, T'(k_0)$ gives the stability of nodes on either side of the Hopf. Combining this with the fact that the limit cycle surrounds a node of opposite stability, we then have our claim. □

Note: Plugging in k_0 and $T(k_0) = 0$ to the formula $(T(k) \pm \sqrt{(T(k)^2 - 4D(k))})/2$, we actually know the values of the eigenvalues at the Hopf bifurcation: $\pm i\sqrt{D(k_0)}$. The period of the eigenvalues (by linearization) is 2π over the imaginary part at an equilibrium. Thus the period of the spiraling at the Hopf point is $2\pi/\sqrt{D(k_0)}$.

Note: The formula for L, as reprinted in [48], p. 353, contains an error and an omission. The error is that the term $a_{11}b_{20}$ at the end of the first line of the equation is reprinted in [48] to be $a_{11}b_{02}$, which basic calculation shows can cause the formula to change sign under

scaling transformations (i. e., $x \mapsto cx$ with c a positive constant). The omission is that [48] fails to indicate the stipulation in [3] that this formula only works as a third derivative along a certain horizontal segment, as described above. This omission is not relevant for determining stability.

Definition 2. *The word criticality is used to refer to the stability of the limit cycles formed at a Hopf bifurcation. If the limit cycles are stable, the bifurcation is supercritical. When the limit cycles are unstable, the bifurcation is subcritical.*

We now include some other theorems that were useful for the implementation of our limit cycle continuation. In our next theorem, we find a bounded region that must contain all limit cycles.

Theorem 4. *Let parameter values for* (2.4) *be given and let R be the open rectangle in (x, y)-space bounded by the lines $x = 0, y = 0, x = 1, y = b/d - 1$. Then any limit cycle(s) of* (2.4) *that lies partially in P must lie entirely within R.*

Proof. We first note that along the x-axis, $\dot{x} = -h$ and along the y-axis, $\dot{y} = -k$, so that there is no flow in forward time from these axes to the interior of P. Thus, any limit cycle that lies partially within P, must lie entirely within the interior of P. (The axes themselves may not contain a limit cycle since they are one-dimensional and do not form a closed loop.) We may now restrict our attention to the interior of P, and it suffices to show that a limit cycle entirely within the interior of P must lie entirely within R. We show this by showing no orbit can cross in forward time the two line segments from R to $\delta P - R$. When $x = 1, x(1-x) \leq 0$, so, in the interior of P, $\dot{x} = x(1-x) - axy/(x+y) - h < 0$, meaning there is no flow in forwards time out of R across the line where $x = 1$. Finally, straightforward calculations show that if $y = x(b/d-1)$ and $0 < x < 1$, then $\dot{y} = y(-d+bx/(x+y)) - k < 0$, and there is no flow in forward time out of R across this line segment either. □

In the next theorem, we find that a path of limit cycles must terminate either at a set including an equilibrium point or at $k = 0$ (which for our purposes is the end of the path, although theoretically some of these paths could be continued).

Theorem 5. *Consider* (2.4)*, and treat* a, b, d*, and* h *as fixed, and consider a path of limit cycles formed at* H*, a Hopf point with* $k > 0$*. This family of limit cycles must approach* $k = 0$ *or terminate at a set including an equilibrium of* (2.4)*.*

Proof. Consider a path of limit cycles where the parameter k does not approach 0. Then there is some $k_{min} > 0$ achieved on the path. By Theorem 4, any limit cycle is contained in the open set R (which does not depend on k) in which (2.4) is analytic. We begin by showing that the path of limit cycles does not approach the point $x = y = 0$, where (2.4) is not analytic. From [57], the system without the harvests (2.3) is continuous at $x = y = 0$ with $\dot{x} = 0$ and $\dot{y} = 0$. Thus, there is some ball, B, around the origin where $\dot{x} > -1$ and $\dot{y} < k_{min}/2$, and we can choose B to exclude the Hopf point. Since (2.3) is obtained from (2.4) by subtracting h and k, as long as $k \geq k_{min}$, $\dot{x} < -1 - h \leq 1$ and $\dot{y} < k_{min}/2 - k \leq k_{min}/2 - k_{min} = -k_{min}/2$. There is, within B, some line segment, l, of slope $-2/k_{min}$ that connects the x- and y-axis. For any $k \geq k_{min}$, the flow of (2.4) across l is given by $\dot{x} - \frac{2\dot{y}}{k_{min}} < 1 - 1 = 0$. Thus, the flow across l is always toward the origin in forward time, and by arguments similar to Theorem 4, there is no limit cycle that crosses l. Since our initial Hopf point was outside of B which contains l, l serves as a bound preventing the path of limit cycles from approaching the origin.

Now we can limit our consideration to a set where (2.4) is analytic, and, by the Planar Termination Principle in [47], a family of one-parameter limit cycles in an analytic planar system must terminate in one of the following ways: the parameter or the cycles become unbounded, the limit cycles approach a critical point, or the limit cycles approach a (possibly compound) separatrix cycle. As defined by [47], a separatrix cycle is a homoclinic orbit (and the equilibrium on the orbit). A compound separatrix cycle is a cycle of connected heteroclinic orbits (and the saddle equilibria they connect). Any separatrix contains an equilibrium, so it suffices to rule out the case where the parameter or the limit cycles become unbounded. The limit cycles may not be unbounded since they are contained in R, by Theorem 4. We now show that limit cycles cannot exist for sufficiently large k,

specifically when $k > b$. Since $-d < 0, \dot{y} = y\left(-d + \frac{bx}{x+y}\right) - k < \frac{bxy}{x+y} - k$ in R. Since $\frac{bxy}{x+y} < bx < b$ in R, $\dot{y} < b - k$ on a periodic orbit. Since any limit cycle must contain some point where y is increasing, no limit cycles can exist when $k > b$. □

Note: Paths can also change direction in k. Generically, this bifurcation is known as a saddle-node of an invariant circle, and is discussed more below.

Note: "Approach a critical point" as used here and in [47] means collapse in size to a single point. Since the continuation of the node from the Hopf point cannot cross outside the limit cycle, the limit cycle must collapse to this continuation (although the continuation of the node may reverse direction in k at values where the continuation of the limit cycle does not reverse direction). Also note that any (compound) separatrix cycle contains a saddle point. These two possibilities correspond to the two manners of destruction that our code checked for, as seen in the next section. Generically, they are Hopf and homoclinic bifurcations.

2.5.2 Implementation in MATLAB

We now describe how we numerically continued the limit cycles formed on the Hopf surface. We will describe the grid we overlaid on the Hopf surface, and our procedure, implemented in MATLAB, that we used to continue limit cycles. The procedures and functions for this implementation are available online at `mason.gmu.edu/~mcrone`.

We will use the language that the limit cycle is created at a grid point on the Hopf surface, and disappears when our tracking no longer finds a fixed point on the Poincaré section. This terminology of creation and destruction is, of course, completely arbitrary. Our code tracks limit cycles from a Hopf bifurcation to the destruction of the limit cycle, or until $k = 0$. Of particular interest is some relationship of values k_1 and k_0, where k_0 is the k at the Hopf point, and k_1 is the k where the limit cycle disappears, to measure whether a limit cycle persists when the harvest changes. The most natural choice might be $|k_1 - k_0|$, but this difference is not very meaningful, since (2.4) is scale-free and the predator

populations where interesting behavior occurs vary by orders of magnitude, depending on the parameters. Inspired by the ratio discussed in Section 2.4, we considered k_1/k_0, but the Hopf surface includes points where $k = 0$ and this ratio is meaningless. In practice, tiny k-values did, for some points on the Hopf surface, lead to high values for this ratio when the limit cycles were still short-lived. The statistic we chose was $|k_1 - k_0|/y_0$, where y_0 is the y at the Hopf point. By Theorem 4, Hopf bifurcations do not occur on the axes, so this ratio is always defined. Also, it ties persistence to the exploitation rate, a ratio of the harvest to the population, a statistic frequently considered in fisheries management. If this ratio is far from 0, we will say that the limit cycle is persistent. If it is close to 0, we will say that the limit cycle is not persistent. Note that "persistent" as we have defined it is a matter of degree, not a binary trait. We will use the terminology "persistent to 0.02" to mean that this ratio is at least 0.02. For this project, we are interested in how prevalent persistent, stable limit cycles are, as this would indicate that the model predicts asymptotically oscillating behavior in the biological population.

We tracked the limit cycles formed at the Hopf bifurcations of (2.4), using a grid in (x, h, q, y)-space of width 0.03. This width was chosen to keep the total computing time of the procedure in the vicinity of one day. In fact, the code on this grid takes approximately 19 hours. Since there are four dimensions, computing would be expected to be roughly inverse quartic with grid width, so a grid with of 0.01 would have taken about 81 times as long.

From Section 2.5.1, we know that both h and q have bounds: $0 \leq h < 0.25$ and $0 < q < 1$. We place a grid of width 0.03 over these two variables starting at 0 in h and 0.03 in q. Of the four variables h, q, x, and y, h is the only variable where we start on the boundary of our region, since $h = 0$ is meaningful and corresponds to a lack of a harvest. All other variables start one grid width in from the boundary. For any h, we have bounds in x, and we establish grid points in x using the width 0.03. Fixing h, q, and x bounds y, and we place a grid on y in the same manner. In each variable except h, we start one grid point away from the lower bound.

In a few cases, points fell exactly on the upper bound, where the value of b goes to 0 or infinity. Due to rounding error, the computer would attempt a value of b in the hundreds of trillions or near the machine epsilon. Remember, from (2.16), the formula for b is a rational function of x, h, q, and y. We inserted code checking for a very small numerator or denominator. Our cutoff was derived based on the orders of magnitude that could be expected to be seen. Consider first the numerator. We chose our cutoff based on the order of magnitude of our grid width (E-2) and the degree of the numerator as a polynomial in x, h, q, and y (cubic). With these in mind, we chose a number less than $(1\text{E-}2)^3$=1E-6. In fact, we chose 9E-7. For similar reasons, our cutoff for the denominator was 9E-9, since the denominator is a quartic polynomial.

For each Hopf point, we conduct natural continuation in the parameter k. Once we have a Hopf point, we track the limit cycle by the procedure given below. We provide our choice of algorithm constants in the line by line notes after the algorithm. We also provide a brief summary of the algorithm after that.

Data: $ODEsystem$, Hopf point: (k_0, x_0, y_0), *nodeprime* (derivative of the node with respect to k), *direction* (left= -1, right= 1), *stability* (unstable= -1, stable= 1)

Result: k_{end} (the k-value where limit cycle disappears)

Initialize *node* to (x_0, y_0)

Initialize k_{old} to k_0

5: Initialize s_{old} to 0

Initialize $fence$ to $Inf * direction$ ($fence$ indicates a value has been checked and no limit cycle was found. We do not let k pass $fence$ in future steps.)

Initialize *grewmore* to 0 (*grewmore* will increase by 1 each time we find a limit cycle and move on to a new k-value. We loop again if this happens every iteration, since we have not seen the end of the path.)

Initialize δk to $direction * k_{error}$ (k_{error} is our error tolerance: heuristically, not analytically.)

Initialize k to $k_0 + \delta k$

for $i = 1 : 1$:maxindex **do**

Let $nodeguess = node + \delta k * nodeprime$

Algebraically find all equilibria of $ODEsystem$ with parameter k

if less than 2 equilibria **then**

Let $s = 2*\text{sign}(s_{old} - s_{closetohopf})$

else

Let $node$ be the closest equilibrium to $nodeguess$

Let $saddle$ be the closest distinct equilibrium to $node$

Let s be the fixed point of the Poincare map scaled to [0,1] on the line segment from $node$ to $saddle$, or 2 if none exists

end if

if $s < s_{old}$ **then**

if $s < s_{tiny}$ **then**

Check numerically for a Hopf bifurcation, H_{end}, for a parameter value near k

if H_{end} exists **then**

Let k_{end} be the k-value at H_{end}

break

end if

end if

Let $s_{target} = \min(s/2, s_{nearnode})$

Let $k_{target} = (k - k_{old})/(s - s_{old}) * (s_{target} - s_{old}) + k_{old}$ (Extend linearly to where s would be s_{target}.)

if $|k_{target} - k|$ is outside the interval $[k_{error}, 2 * k_{error}]$ **then**

Adjust k_{target} so $|k_{target} - k|$ falls on the closest endpoint of $[k_{error}, 2 * k_{error}]$

end if

if $k_{target} < 0$ **then**

Let $k_{target} = 0$

end if

if $k_{target} * direction > fence * direction$ **then**

Let $k_{target} = (fence + k)/2$

end if

else

if $s > 1$ **then**

Let $k_{target} = (k + k_{old})/2$

Let $fence = k$

else

if $s < s_{nearsaddle}$ **then**

Let $s_{target} = (s_{nearsaddle} + 1)/2$

Let $k_{target} = (k - k_{old})/(s - s_{old}) * (s_{target} - s_{old}) + k_{old}$ (Extend linearly to where s would be s_{target}.)

if $|k_{target} - k| > 2 * k_{error}$ **then**

Adjust k_{target} so $|k_{target} - k| = 2 * k_{error}$

end if

if $k_{target} < 0$ **then**

Let $k_{target} = 0$

end if

if $k_{target} * direction > fence * direction$ **then**

Let $k_{target} = (fence + k)/2$

end if

else

Let $s_{target} = 1$

Let $k_{target} = (k - k_{old})/(s - s_{old}) * (s_{target} - s_{old}) + k_{old}$ (Extend linearly to where s would be s_{target}.)

if $|k_{target} - k| < k_{error}$ **then**

if $k_{target} * direction > fence * direction$ **then**

Let $k_{target} = (fence + k)/2$

end if

$k_{end} = k_{target}$

break

else

$k_{target} = k + direction * k_{error}$

if $k_{target} * direction > fence * direction$ **then**

Let $k_{target} = (fence + k)/2$

end if

end if

end if

end if

if $s < 1$ **then**

Let $k_{old} = k$

Let $s_{old} = s$

Let $grewmore = grewmore + 1$

end if

Let $k = k_{target}$

Let $\delta k = k - kold$

if $grewmore = maxindex$ **then**

Let $i = 0$ (start the for loop over)

end if

end for

Line 1: Note that all these inputs are known. Our Hopf point is our grid point, *nodeprime* is based on standard multivariate calculus, *stability* from (2.17), and *direction* from Theorem 3.

Line 8: The variable k_{error} is a heuristic error bound, since we do not in later steps

predict the destruction of a limit cycle unless we expect to be within k_{error} of the destruction. We set value k_{error} is set to max $\{(1\text{E-}2)k_0, (1\text{E-}4)y_0\}$. Initially, we only we set a value based on $k, (1\text{E-}2)k_0$, which represents a goal of being close (within 1%) in k, but the second y_0-based bound was added to allow larger steps when k_0 was tiny.

Line 10: We chose $maxindex = 26$. This value was chosen so that paths which decrease in k without approaching either node or saddle will reach $k = 0$ in 2 for loops. Initial attempts with $maxindex = 51$ (which would reach $k = 0$ in one for loop) had a runtime error for some points for which δk reached 0 in machine arithmetic. The smaller value $maxindex = 26$ did not have this error.

Line 12: In our code, we eliminate equilibria not in P. Because of machine epsilon issues, we ignore imaginary parts smaller than 1E-8. We chose 1E-8 because it is near the order of the square root of machine epsilon.

Line 14: We will see later that s is a value between 0 and 1 when a limit cycle is found. Here we assign ± 2 to s as a flag that no equilibrium exists. The value $s_{nearnode}$ represents a value below which our fixed point is close enough to the node that destruction in a Hopf bifurcation is expected if the equilibrium disappears. We chose $s_{nearnode}$ to be 0.2.

Line 17: Again, we use the constant 1E-8 to correct for machine epsilon issue. We let *saddle* be the closest equilibrium outside a ball of radius 1E-8 in the infinity norm of *node*.

Line 18: Since (2.4) is a planar system, there is one time direction in which orbits will be attracted to the limit cycle initially. We ran simulations in that time direction, which we determined using the formula from Theorem 3. We used a Poincaré section based technique to search for limit cycles. For any given k, we searched along the line segment in phase space between *node* and *saddle* using MATLAB ode45 with an event function that found when (if at all) the orbit intersects again the line through *node* and *saddle*, while the orbit was crossing in the same direction as it was initially. For any point s on the line, I will call this return point $P(s)$. If the orbit does not intersect that ray after for $20\pi/\sqrt{D(k_0)}$ time units, the code stops. Recall that $2\pi/\sqrt{D(k_0)}$ is the period of the limit cycle near H. We chose this upper bound to be an order of magnitude higher than the initial period.

Our code makes an adjustment to the default settings of ode45 and two other changes in the implementation. One is to change the relative tolerance to 1E-5 (from a default of 1E-3). Our reasons for this change are discussed later in this section. The other is to add a nudge of (2E-3)$\pi/\sqrt{D(k_0)}$ time units to prevent MATLAB from stopping integration in ode45 immediately because the starting value is on the line. Only a very small nudge was needed, so we chose 3 orders of magnitude below the initial period. Recall that limit cycles cannot leave the rectangle R by Theorem 4. As implemented in MATLAB, my code adjusts (2.4) to stop an orbit when either x or y falls more than 1E-2 outside of R.

When an orbit fails to return to the line, my code assumes that no limit cycle exists across our test segment at that k-value. When an orbit returns to the line, we try another point along the segment, which we will call s_{n+1}. If $P(s_n)$ moves towards node from s_n, we try s_{n+1} closer to *node* than s_n. If $P(s_n)$ moves towards *saddle* from s_n, we try s_{n+1} closer to saddle than s_n. If $P(s_n) = s_n$, the search stops and returns s_n as a fixed point. In practice, exact equality has not been observed after the nudge was introduced to eliminate improper stopping of ode45.

In this way, we conduct a binary search for the fixed point associated with the limit cycle. In our code, the search goes for 7 steps, so the error associated with the binary search at most $1/128^{th}$ the length of the line segment. In this way, for any k, our code returns a fixed point, if (our code believes) one exists, that we will call s, that matches the stability of the limit cycle. In coding, and in what follows, we associate s with a real number between 0 and 1, representing the proportion of the way from node to saddle that the fixed point occurs with 0 being *node* and 1 being *saddle*.

Note on how we came up with the relative tolerance we used in the "options" set for our code: Our method is dependent on ode45 being sufficiently accurate to determine whether orbits are spiraling in or out from the node. At the default relative tolerance, there were a lot of orbits which spiraled in ways inconsistent with theory (crossing orbits, etc.). A test was derived using the 50 grid points of the case where $x = 0.45, h = 0.09$, and y and k vary on a grid with width 0.06. This slice of the Hopf surface was chosen, because the limit cycles

formed on this slice showed a variety of behaviors in terms of stability and persistence. At each of these 50 grid points, we considered 9 values of k evenly spaced along the interval from k_0 to a rough guess of k_{end} using the estimates for the first derivative on a limit cycle in [48] and the third derivatives of Poincaré map from [3] (even though these derivatives are for a different line segment than we use). We then found the value of the Poincaré map at the point where $s = 0.01$, to provide us with a start point near the node. Some of these k-values were negative, and were not used. All positive k-values were tested, and there were at least 300 of these. Using the default tolerances, all MATLAB ode solvers showed some failure to get the spiraling direction correct. However, with a relative tolerance of 1E-4, one order of magnitude more fine, ode45 got the right spiraling direction for all points. That is, for all points that spiraled in the wrong direction based on the stability of the node near the known Hopf, it could be found algebraically using MATLAB's solve that another Hopf occurred on the same branch, reversing the stability of the node (and ode45 with this tolerance was actually right). However, we brought the relative tolerance down to 1E-5 and instituted the algebraic Hopf finder using solve, when we found one point (using a different k than in the test) where the direction failed to be correct near a Hopf point with s_n slightly more than 0.01. With the new relative tolerance, the spiral direction became accurate for this value.

Binary search was chosen here because it has known error bounds, and because Newton's Method had several difficulties including the inexactness of a derivative found using ode45 and the tangent method, convergence to the fixed point at $s = 0$, and attempted iterates outside the interval [0,1]. Binary search and natural continuation also seemed, in practice, to reduce the number of calls to ode45, speeding up the code.

Line 21: Some points fail to be accurate when tested at smaller values of s_n than 0.01, which is why we test for destruction at a Hopf whenever $s < s_{old}$ and is less than 0.02, since $0.02 > 0.01 + 1/128$. (1/128 is the error of the binary search.) Thus, we use $s_{tiny} = 0.02$.

Line 22: Near, in this context, is taken to be within $3k_{error}$. This constant was chosen because it smallest value that will detect almost immediate destruction in a Hopf bifurcation

based on our algorithm. We check for a Hopf by numerically solving the algebraic Hopf conditions of the Jacobian (trace is 0, determinant is positive) using MATLAB's solve command.

Line 44: We chose $s_{nearsaddle}$ to be 0.8, since we decided observing a limit cycle crossing in the last 20% of the line segment was close enough the reaching the saddle point that we would report a homoclinic bifurcation if, by linear extension, one was expected that was close in k.

Summary of algorithm

In sum, we begin at a known Hopf point H, a grid point on the Hopf surface. Based on Theorem 5, the path of limit cycles emanating from H, if it terminates without reaching $k = 0$, may only do so in two ways: collapsing back to the node that is the continuation of H or expanding to touch another equilibrium. We begin by finding the nearest equilibrium. We then see how far along the line segment to the node the limit cycle crosses. If it's close enough to the node, we check the algebraic Hopf conditions for a nearby Hopf point. If it's close enough to the saddle, we extend linearly to where we expect to hit the saddle. If we somehow pass the k-value when the limit cycle disappears, we use fence to not pass that value again.

Note that the code does not search for a change of direction in k. This omission is real, but is justified for our system (2.4) by the numerical comparison in the next section.

2.5.3 Comparison to results from AUTO

We verified the results of this limit cycle tracker using a grid of width 0.12, because this grid had only 82 points, which was tractable for the manual checks we discuss below. Also, because 0.12 is a multiple 0.03, with this choice of grid width, our test grid points will also be points on the larger grid. Our values for these points were compared against those obtained by AUTO [24], a commonly used dynamical systems software. AUTO continues limit cycles by a completely different method than our MATLAB procedure. Whereas we

continue limit cycles by the Poincaré section technique described above, AUTO converts the continuation problem to a boundary value problem where the period of the limit cycle becomes one of the parameters, and discretizes the boundary value problem. The other difference is that our technique conducts natural continuation, meaning continuation in a single parameter (k), whereas AUTO conducts pseudo-arclength continuation in the period of the limit cycle and one of the parameters (which we chose to be k). Specifically, given a Hopf point or a limit cycle, AUTO finds a solution to the boundary value problem where a weighted magnitude of the change in both k and the period is within some step size. Of note, in our practice, if this step size was too small, AUTO would not find the limit cycle and would return a "continuation" consisting of k-values very close to the Hopf point, with the period changing.

We did not have success in AUTO starting our limit cycle tracking at the Hopf surface, instead we needed to adjust the Hopf point by finding a nearby equilibrium and then letting AUTO find the Hopf point. Instead of re-creating our quartic solver in AUTO, we found an equilibrium by replacing the x at the Hopf point with $0.99x$. The value of $0.99x$ was chosen because it provides a slight nudge and allows AUTO to find the Hopf point, but, did not, in practice, introduce any other topological change that we observed between the start point and the Hopf point.

Given $0.99x$, finding the corresponding y and k becomes a linear system, which we used to find an equilibrium at $0.99x$. Then we searched for a Hopf point by increasing k. That an increase in k bring us back to our Hopf point is known by Lemma 3. This is also a continuation procedure in AUTO and finding the Hopf point depended on step size just as the limit cycle tracking did. If the step size was too large, AUTO would skip over the Hopf point and not find it.

From the previous few paragraphs, we have conditions requiring us to fine-tune the step size. If the step size was too small, AUTO would not find the limit cycle and if the step size was too large, AUTO would not find the Hopf point. The step size in AUTO is adaptive, but it depends on a user-defined initial step size and minimum step size. No choice of these

two values was found that worked for the entire 82-point grid, but some choice worked at each point, and we were able to find continuations in AUTO that avoided both of these problems for all 82 points.

The results from AUTO confirm the accuracy of our limit cycle tracker. The k-values of the end of the path of limit cycles were within k_{error} on the entire grid, and our persistence ratios for all points matched within less than 0.01. We will show persistence results for the finer grid using our limit cycle tracker in Section 2.5.4. The match to AUTO on the coarse grid is demonstrated here as confirmation of those results. The full results for the comparison on the test grid are posted online at `mason.gmu.edu/~mcrone`.

Even for results where our code found no valid reason for the limit cycle to disappear, our k-value matched those given by AUTO. AUTO frequently finished with a near vertical completion in these cases: that is, the limit cycles grew very fast with respect to x. Figure 2.6 shows the output for a point on the test grid where $x = 0.12, h = 0, q = 0.24$, and $y \approx 0.245$, a grid point for which our code had no known reason for the destruction of the limit cycle. Note the near verticality of the branch representing the limit cycles. The labeled points along the vertical section represent points where the path of limit cycles changed direction in k. Due to verticality, the k where this behavior begins is quite close to the end of the branch. Bifurcation diagrams for some of the other points on the test grid are shown in Figure 2.7.

We found that the saddle-node of the invariant circles were reported in AUTO, but that the end of the bifurcation branch and the end of the range in k where limit cycles were very close to the same value, varying by no more than (3E-4)k. This justifies not considering these bifurcations in our program, although in future work, we propose to search for these using our code.

2.5.4 Numerical Results

We conducted the limit cycle tracking in MATLAB described in the previous section on a grid on width 0.03, a grid that has 31,122 grid points. The results are posted online at

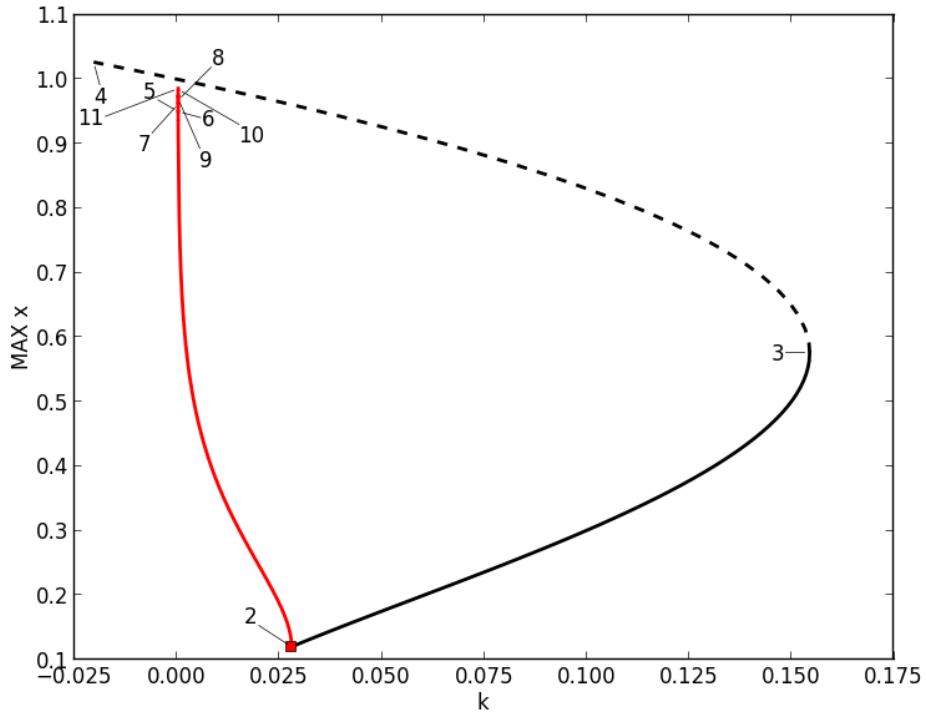

Figure 2.6: A bifurcation diagram created in AUTO for a grid point on the test grid where our code had no known reason for the destruction of the limit cycle.

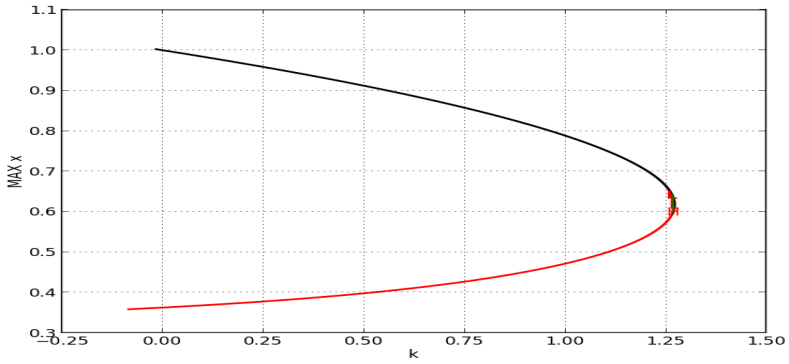

(a) $h = 0, q = 0.12, x = 0.6, y \approx 0.74$

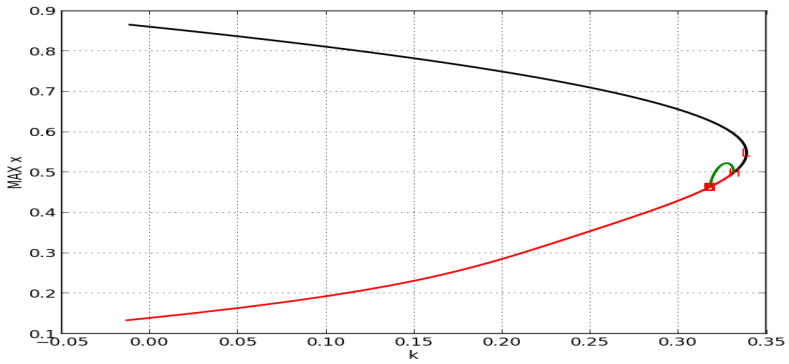

(b) $h = 0.12, q = 0.12, x \approx 0.50, y \approx 0.60$

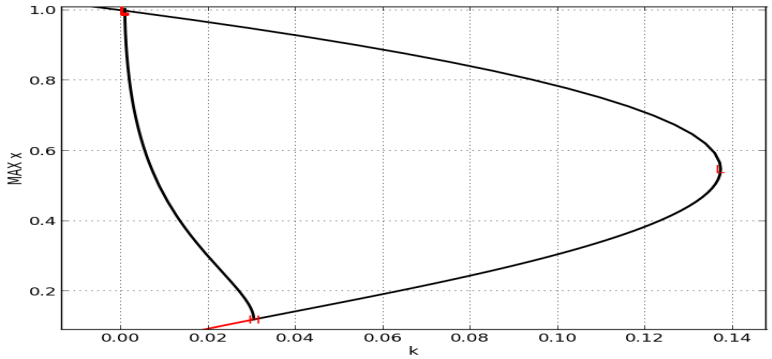

(c) $h = 0, q = 0.12, x = 0.12, y \approx 0.47$

Figure 2.7: Bifurcation diagrams for (2.4) created in AUTO tracking limit cycles on the test grid. The top diagram shows the most typical behavior, a limit cycle that quickly disappears in a homoclinic bifurcation. The middle diagram shows a limit cycle that tracks to another Hopf bifurcation. The final diagram shows a limit cycle we found to be persistent (to 0.06) and stable, the second most persistent stable limit cycle path on the test grid after the parameter choices for Figure 2.6, which we found to be persistent to 0.11.

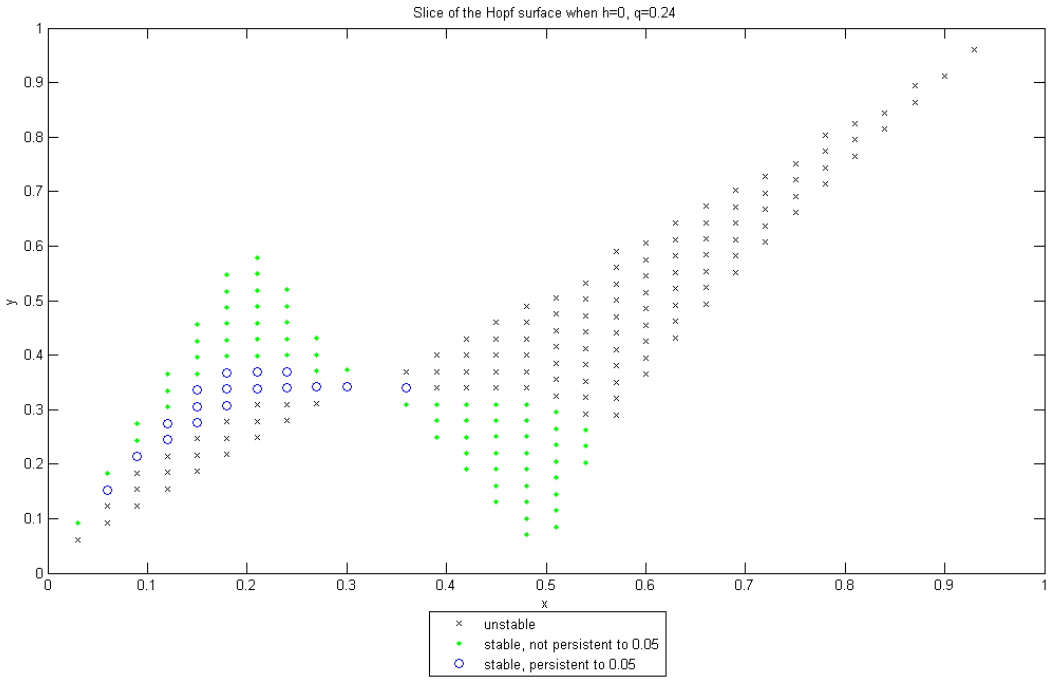

Figure 2.8: Criticality on the slice of the Hopf surface where $h = 0$ and $q = 0.24$, with points forming persistent, stable limit cycles highlighted. This slice contains 205 grid points.

mason.gmu.edu/~mcrone. We found that persistent, stable limit cycles do exist, although they exist primarily when $h = 0$ and were quite rare when $h > 0$.

We will focus in our discussion of the results on limit cycles that were persistent to 0.05, which we motivate in this paragraph. In fisheries science, the exploitation ratio is the proportion of a fish population that is harvested each year. Our persistence ratio would relate directly to the exploitation ratio except for the fact that time in (2.4) is made scale-free by making the growth rate, r, of the prey 1. Returning scale to our model, a limit cycle which is not persistent to 0.05 would represent a population where the small change of $0.05r$ (typically, smaller than 0.05) in the exploitation ratio would represent passing over the entire region of oscillatory behavior. In practice, this is a small change in the exploitation ratio, and, thus, by considering a cut-off at 0.05, we will not exclude any limit cycles of practical relevance.

We found that 232 grid points (0.7%) formed stable limit cycles that were persistent to 0.05, with 226 of these points occurring when $h = 0$. 226 is 3% of the total number of grid points where with $h = 0$ (6,758). The q for these points varied among all values on the grid that were less than or equal to 0.75. (Recall that $q = d/b$ is the ratio that we defined in Section 2.2.3.)

We will visualize the Hopf surface by taking two-dimensional slices in h and q of the four-dimensional surface. The number of grid points on each slice were observed to vary considerably, from a maximum of 1,054 when $h = 0$ and $q = 0.03$, to a minimum of 0 for all slices where $q \geq 0.9$. For any given h, the number of grid points was observed to be nonincreasing in q. For any given q, the minimum number of grid points was always observed to be achieved when $h = 0.21$ or $h = 0.24$, and the maximum achieved when $h = 0$ or $h = 0.03$.

The four-dimensional Hopf surface has hundreds of these slices for our grid width of 0.03. We provide graphs of eight of these slices in this section: four showing the stability and persistence for slices without a harvest (since that is where most stable, persistent limit cycles are formed) and four showing stability and persistence with a harvest. For the graphs

with a harvest, we chose $h = 0.03$, to maximize the number of grid points in the graphs.

Figure 2.8 shows persistence and criticality (see Definition 2) for the two-dimensional slice of the Hopf surface where $h = 0$ and $q = 0.24$, the slice in h and q that shows the most stable limit cycles that were persistent to 0.05. As seen in the figure, the Hopf surface has a pinch point where its height shrinks down to nothing. Numerically, we observe such a pinch point in all slices with a sufficient number of grid points to see the structure of the grid. We also note that a band of stable, persistent limit cycles occurs in the left piece of the slice, extending just past the pinch point. The band is near a curve through the center of the slice where stability reverses. For other choices of q, the picture remains qualitatively similar as long as $h = 0$. The band of stable, persistent limit cycles shifts to the left as q increases, and becomes thinner as q moves either direction from 0.24. When $q \geq 0.66$, subcritical Hopf bifurcations are no longer observed in the left hand side of the slice, and the stable, persistent limit cycles are observed on the lower boundary of the Hopf slice. Plots for $h = 0$ and $q = 0.03$, $q = 0.45$, and $q = 0.66$ are shown in Figure 2.9.

When $h > 0$, we found far fewer stable, persistent limit cycles. In fact, only six (0.02%) out of 24,364 grid points with $h > 0$ formed stable limit cycles that were persistent to 0.05, and no stable limit cycles were persistent to 0.06 with $h > 0$. There is also a qualitative change in the shape of the region where limit cycles are stable with a positive h from the graphs with $h = 0$. The Figure for $h = 0.03, q = 0.03$ is shown in Figure 2.10. Stability in the left hand portion of the surface now appears to depend mostly on x alone, as the curve of stability change is near vertical. For all but one choice of x on the left hand side of slice, stability of limit cycles was not observed to vary with y. When x is small, the limit cycles are stable. Call this apparently connected region of stable limit cycles S_l. When x becomes large enough, as long we remain in the left portion of the slice, the limit cycles are unstable. The right hand portion of the slice remains qualitatively similar for all values of x and h, including those where $h = 0$. Keeping h fixed at 0.03 and increasing q, we find that the criticality on the surface follows a qualitatively similar pattern until $q = 0.21$, when a new manifold of stable limit cycles is observed to the right of the unstable ones, but on the left

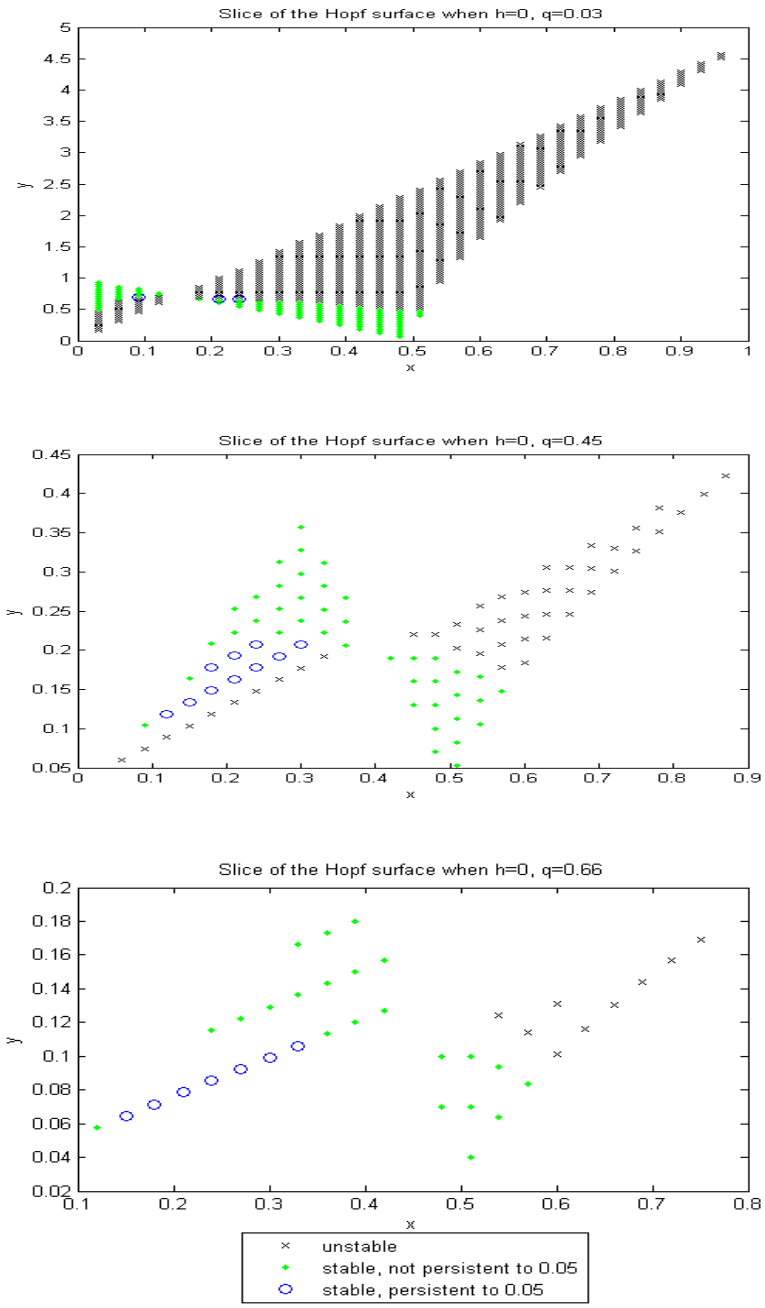

Figure 2.9: Criticality on the slice of the Hopf surface where $h = 0$ and $q = 0.03, 0.45$, and 0.66 from top to bottom. Points forming persistent, stable limit cycles are highlighted.

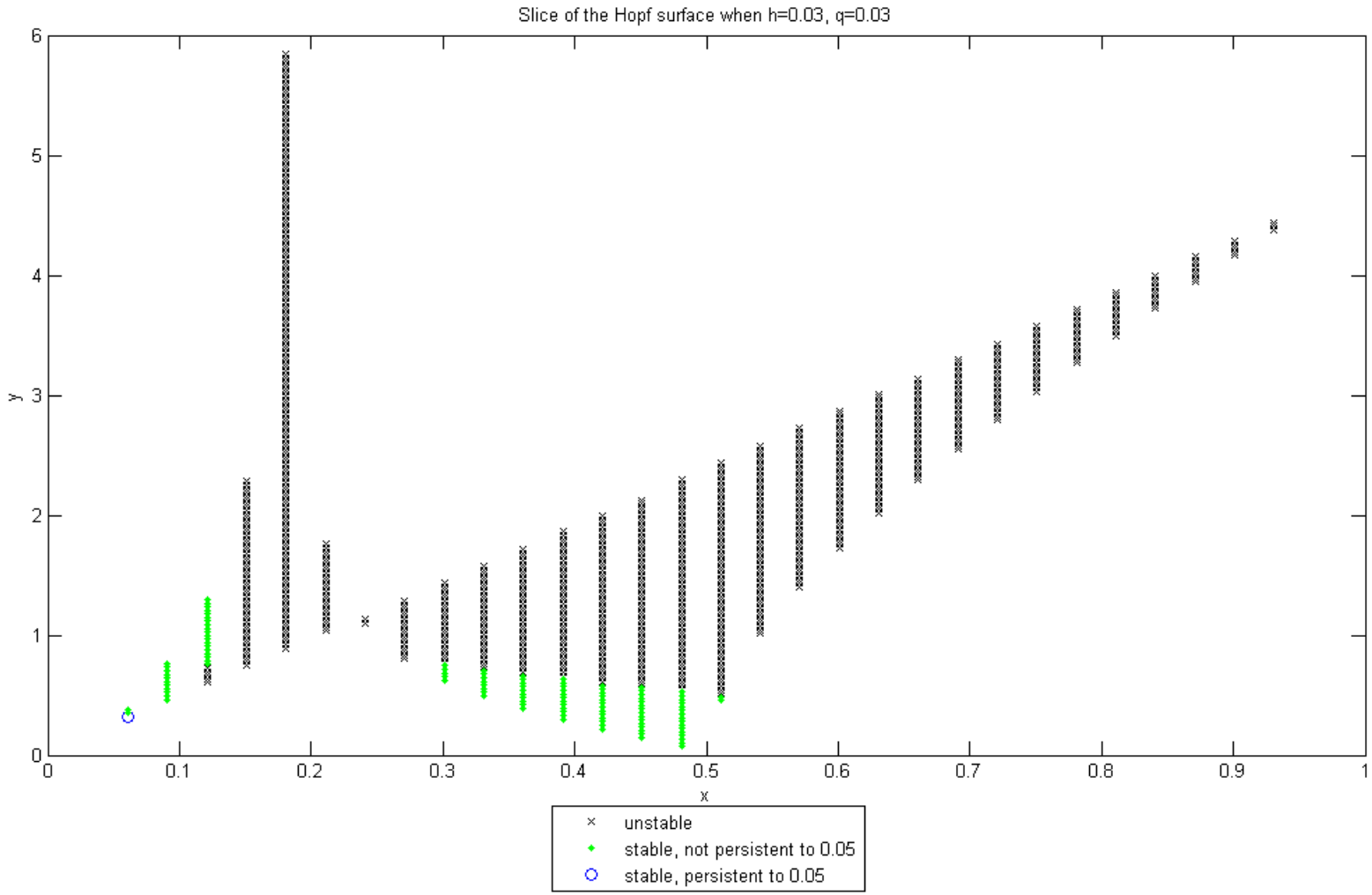

Figure 2.10: Criticality on the slice of the Hopf surface where $h = 0.03$ and $q = 0.03$. The single grid point forming a persistent, stable path of limit cycles is highlighted on the bottom left.

side of the slice. We will call this new region S_c. As q increases further, the boundary of S_c becomes less vertical, and the boundary the region S_l becomes smaller until by $q = 0.54$, S_l is no longer observed. (See Figure 2.11.) As S_l approaches the point on the left hand side of the Hopf slice, it becomes difficult to ascertain whether the boundary of S_l remains near-vertical due to the lack of grid points. With larger values of h as well as q, it appears that this boundary as well is losing its verticality. As q increases further, the slices remain qualitatively similar until they contain few enough points that features cannot be discerned. For other positive values of h, the behavior as q changes is similar in terms of S_l, which the region shrinking as q increases, but by $h \geq 0.15$, S_l is not observed to disappear until the slice has 25 or fewer grid points, when it becomes difficult to discern the slice's features. The region S_c is more intermittent for larger h, and is not observed for any q when $h \geq 0.15$.

In summary, we find that stable limit cycles are only persistent to changes in the predator harvest when the prey harvest, h, is small. Almost all observed stable, persistent limit cycles occurred when h was 0. Given that equilibrium population of the prey is 1 in the absence of predation or harvest, the minimum positive harvest considered of 0.03 is relatively small. While stable limit cycles are possible with a positive prey harvest, they appear to be an unlikely phenomenon. Further investigation of the region where h is small is needed.

2.6 An observation regarding predator harvesting

Suppose a, h, d, and b are fixed and consider (2.4) with k as varying. We have numerical indications that show that several qualitatively different bifurcation schema (in k) are possible for our system, depending on our choice of the other parameters. For simplicity, we will only consider a, h, d, and b that satisfy conditions (3.ii) or (3.iii) of Lemma 2.1 in [55], which by simple calculation can be combined into the condition:

$$\frac{b - a(b-d)}{2b} < \sqrt{h} < \frac{1}{2}. \tag{2.18}$$

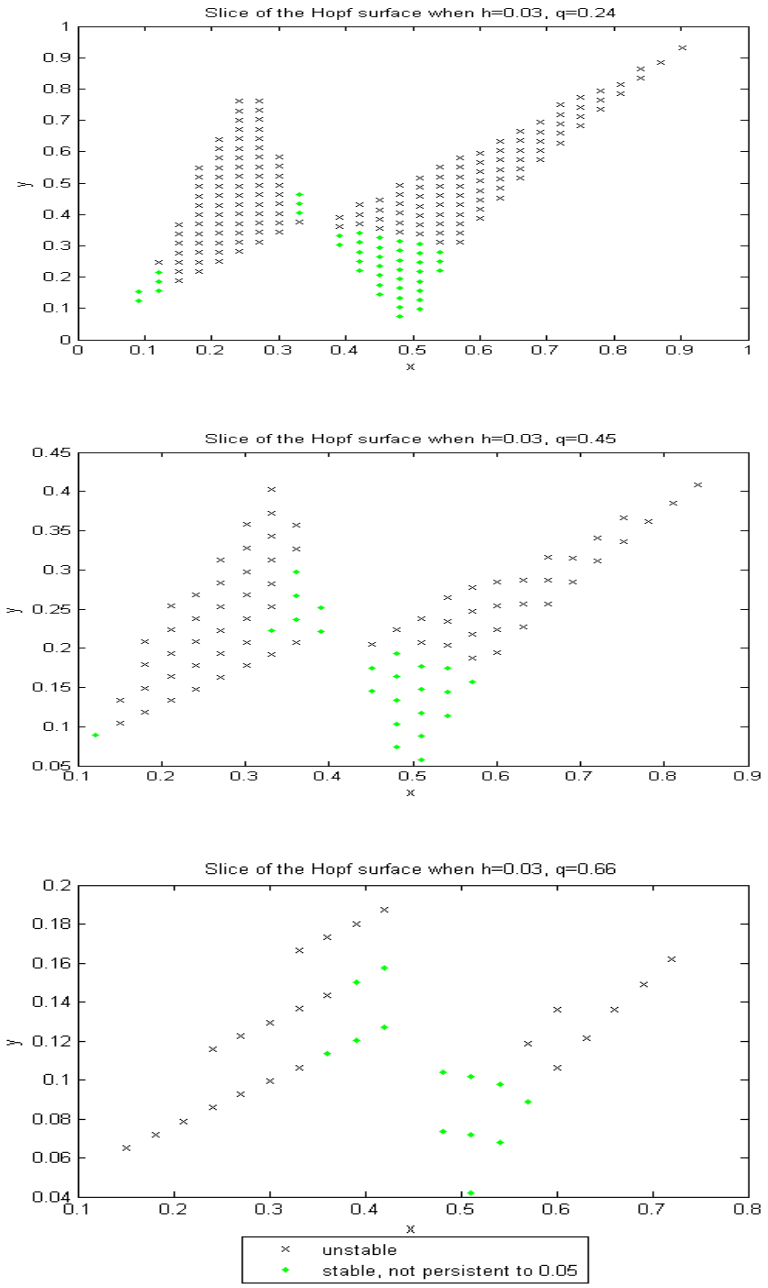

Figure 2.11: Criticality on the slice of the Hopf surface where $h = 0.03$ and $q = 0.24, 0.45,$ and 0.66 from top to bottom. No points formed persistent, stable limit cycles.

Then by that lemma and Theorem 2.3 also in [55], we know that when $k = 0$, all orbits move toward extinction of the predator: they either go to an equilibrium on the x-axis as $t \to \infty$ or hit the y-axis in finite time. In either case, we have $y \to 0$ as $t \to \infty$, since once $x = 0$, we have $\dot{y} = -dy$.

It might be expected that a strictly positive k could not "improve" this result. In other words, keeping a, h, d, and b constant and satisfying (2.18), but using a strictly positive k, it might be expected that predator extinction remains inevitable. However, this intuition only considers the immediate, direct consequences and proves incorrect. We have found several examples of parameter values that show this phenomenon in the model and include one such example here.

It is easily seen that the parameter values $a = 0.6, h = 0.05, d = 5\text{E-}3$, and $b = 1$ satisfy (2.18), so when $k = 0$, extinction of the predator species occurs in (2.4) for any initial condition. However, when $k = 0.3$, linearization shows that the equilibrium that occurs at approximately $x \approx 0.378, y \approx 1.681$ is stable, so it has some region of attraction for which the solution approaches the equilibrium, and extinction is averted. In fact, there is a sizeable region of attraction as seen in the phase portrait in Figure 2.12. This result supports the insight that under certain conditions, culling a resource population may actually improve the long-term health of the population.

2.7 Application to the oyster and black drum fisheries in Louisiana

In this section, we apply (2.4) to the oyster and black drum populations of Louisiana. To match population data to real world data, we must now convert (2.4) out of its scale-free form. With constant harvests, our model becomes:

$$\dot{x} = rx(1 - \frac{x}{M}) - \frac{axy}{x + cy} - h \tag{2.19}$$

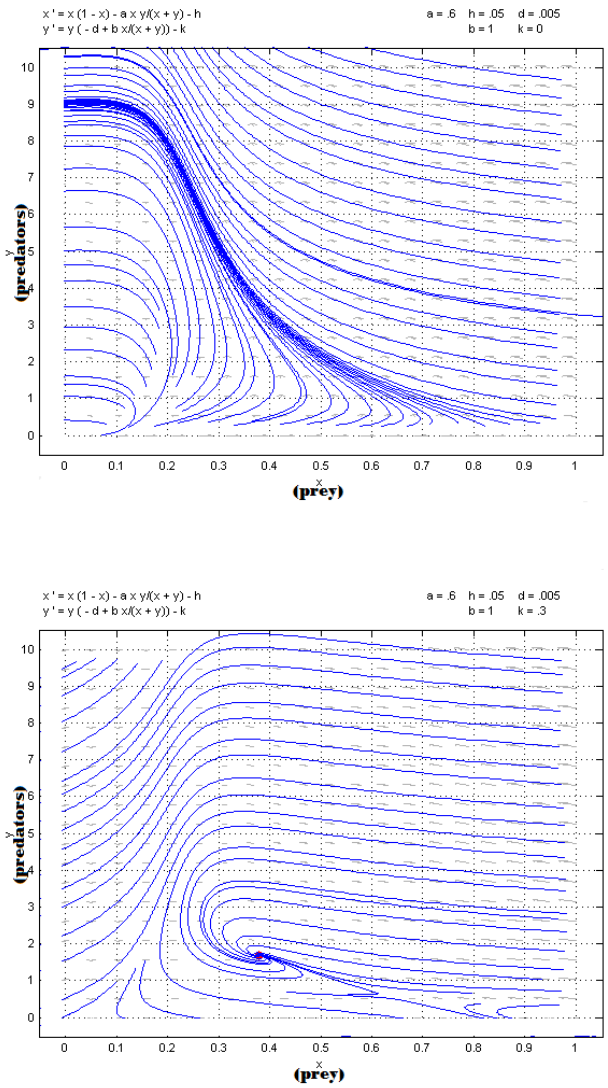

Figure 2.12: Phase portraits of (2.4), the ratio-dependent predator-prey model with constant harvests. The only parameter that is changed from the top portrait to the bottom one is k, representing the predator harvest. In the top one, $k = 0$, and all orbits lead to extinction. In the bottom one, $k = 0.3$, and some orbits approach a stable equilibrium (red dot) and extinction is averted.

$$\dot{y} = y\left(-d + \frac{bx}{x + cy}\right) - k.$$

We modeled the period 1986-2008 inclusive, the longest period for which landing and population data were available for both species. In reality, harvest of neither species was constant over the period. We used harvest data to find the h and k for each species each year. While in theory this should remove both constants from the model, in reality, proportionality constants returned for each species due to reasons described below, and our system becomes:

$$\dot{x} = rx(1 - \frac{x}{M}) - \frac{axy}{x + cy} - hc_{1,t} \tag{2.20}$$

$$\dot{y} = y\left(-d + \frac{bx}{x + cy}\right) - kc_{2,t},$$

where the constants $c_{1,t}$ and $c_{2,t}$ with t a year between 1986 and 2008 are the harvest data.

In consultation with Dr. Kim DeMutsert of the George Mason University Environmental Science and Policy Department, black drum and oysters were chosen as an approximation to a pure predator-prey system for which population surveys and landing data were available. For oysters, we obtained population and landing data from [44]. For black drum, we obtained population and landing data from [9]. We will discuss each population and the data available in the next two paragraphs.

Louisiana contains both public oyster grounds and private leased waters where oysters are harvested [44]. The public oyster grounds are harvested for small oysters, known as "seed" oysters: oysters smaller than three inches which are moved to private leases. There are also large oysters, those greater than three inches, which are known as "sack" oysters, and are taken directly to market. Population estimates are available in [44] for both types of oysters. We use the total oyster population from Figure 4 in [44]. We convert these figures to numerical data using the tool, WebPlotDigitizer [52], available online. These surveys are

conducted during the summer [22]. We treat the populations as point estimates occurring in the midpoint of the each. Landing data are only presented in [44] for sack oysters. For this reason, we assume that seed oyster removal from the public grounds was proportional to sack oyster removal. The constant of proportionality is a parameter that we fit to the data, by leaving the harvest rate unknown. The landing data given in Figure 3 in [44] are again converted using WebPlotDigitizer.

Black drum in Louisiana are harvested both commercially and recreationally [9]. We used the total harvest from an unnumbered figure the executive summary in [9] for the harvest in our model. For population estimates, we modeled population as proportional to catch per unit effort in trammel net surveys conducted by the Louisiana Department of Fish and Wildlife and shown in Figure 6 in [9]. Although we could not find documentation of the timing of the estimates, the most likely case based on [22] is that they occur year-round. As an approximation, we used them as point estimates for the midpoint of each year. Again, these figures were converted to numerical data using WebPlotDigitizer.

2.7.1 Parameter estimation: methods

In implementation, we first normalized our population and harvest data so that the average for each of the four data sets is 1. We seek to minimize a normed difference between observed and calculated data, specifically:

$$\sqrt{\sum_{t=1987}^{2008} \left(x_o(t) - x_c(t)\right)^2 + \sum_{t=1987}^{2008} \left(y_o(t) - y_c(t)\right)^2}, \tag{2.21}$$

where $x_o(t)$ and $y_o(t)$ are the observed population at time t, and $x_c(t)$ and $y_c(t)$ are the population values obtained by taking the population observed in the previous year and running the ODE (2.19) in ode45 for one year. We then estimated the parameters for our data by a three-part procedure:

- We found 20 sets of parameters that will not cause either population to soar or crash

within one year,

- We use particle swarm optimization (described below) to find parameters that match the data, and
- We use method of steepest descent to further refine our parameter estimate.

We discuss each of these steps in the following sections. This gave us a set of parameters optimized to our data. Because of the random elements in the procedure, it can be repeated and, at least potentially, achieve different results. We found 50 sets of parameters which we compare in Section 2.7.2.

Initialization of parameters

We find a set of initial parameters in the following way: For each parameter, we chose a random number, s, from a uniform distribution on [0,1], and set the parameter to $s/(1-s)$, which translates [0,1] to $[0,\infty)$. We will adjust this choice to parameter values such that both the oyster and black drum populations stay within the interval $I := [0,3]$ for one year. We chose $[0,3]$ for I since it was the smallest integer interval that the actual data stayed within. We ran 22 one-year simulations of the model using ode45 starting from each of the 22 data points corresponding to the observed populations in 1986-2007 inclusive. If none of the simulations fell outside I, our current parameter estimates would be good enough to be considered initial data for the particle swarm optimization. If not, we would consider the year where a population left I the fastest. There are four possibilities for how the population left I : $x < 0, x > 3, y < 0$, or $y > 3$. Suppose x falls below 0. We want to increase x. There are four parameters that relate only to $x : r, M, a$ and h. The formula for $\dot{x}$ increases with r and M and decreases with a and h. We choose one of these parameters at random and change it by multiplying it by a random number. We choose our random number from [0,1] if we want the parameter to go down, and we choose our random number from [1,2] if we want our random number to go up. In this way, we change a parameter in a way that (naively, at least) increases x and try again. Similarly, if $x > 3$, we make a

parameter change to decrease $\dot{x}$. If y falls outside I, we similarly use the parameters b, d, and k, and the fact the $\dot{y}$ increases with b and decreases with d and k. Trials runs indicated that this procedure found an initial point within 50 steps over 95% of the time. We set our code to stop after 100 steps to avoid long delays.

Particle Swarm Optimization

Particle swarm optimization is a nonlinear optimization technique motivated by a model of human behavior [40]. We chose particle swarm optimization because it was convenient, and when we tried it, we got good answers, but this technique has no known performance guarantees. In our implementation, each of the 20 parameter choices represents a "particle" which moves about parameter space searching for a point that minimizes (2.21). We number the particles from 1 to 20, and define the neighbors of a particle to be those within 1 of the particle mod 20. Particles will act based on the point in parameter space where either the particle or its neighbors have been that minimized the objective function (2.21), in the manner described below. The movement of each particle is given by:

$$0.7298\eta + U(0, 1.4961)(p_i - \alpha) + U(0, 1.4961)(p_g - \alpha) \mapsto \eta$$

$$\alpha + \eta \mapsto \alpha,$$

where η is particle's velocity, α is the particle's position, $U(m, n)$ is a uniform distribution on $[m, n]$, p_i the position where the particle has seen the lowest value of the objective function, and p_g is the position where the minimum value of the objective function has been observed by either the particle or its neighbors. We move the particle through parameter space according to this formula for 100 steps. At each step, we evaluate (2.21), and update each particles p_i and p_g as appropriate. At the end of the procedure, the location in parameter space where the lowest value of (2.21) ever observed is retained and refined further by the method of steepest descent as discussed in the next section. The choice of function was based on [40], which indicates that this formula has been standard since the analysis in [18].

The definition of neighbors varies in usage, and can even expand in implementations in other settings to where all particles are neighbors. As indicated in [40], larger neighborhoods are more subject to getting stuck in local minima.

Method of Steepest Descent

Finally, we refine the parameter choices further by a form of the method of steepest descent, which we describe in this section. We begin with initial parameter choices $p_0 = \{a_0, b_0, c_0, d_0, h_0, k_0, M_0, r_0\}$ and evaluate (2.21) at these points. We then evaluate (2.21) at each of 16 points, changing one parameter at a time by 1% in each direction. The 1% changes were chosen to represent a small nudge each step. If, for a given parameter, (2.21) increases when that parameter is increased and increases as well when it is decreased, we do not change that parameter that step. If one of the changes results in a decrease of (2.21), we move that parameter in the direction of the decrease. We then change our parameter choices by the formula $p + \gamma \cdot p \mapsto p$, where γ is a vector of norm 0.01 whose nonzero entries are proportional to the derivate of (2.21) with respect to γ as determined by the tangent method and the values when multiplying the current value by 0.99 and 1.01. (On the off chance that the value of (2.21) decreases in both directions, we use twice the minimum decrease in the direction of the maximum decrease.) In this way, we have our next iterate, and we continue for 50 steps in this way.

2.7.2 Numerical Results

Since the procedure described above contains stochastic elements, different runs of the procedure can give different results. As indicated above, we ran the procedure 50 times. We found that while the value of the objective function was quite similar for most runs and the predicted forward orbits using the parameters given were rather similar for each run, the actual values of the parameters chosen showed a large amount of variation over the runs. This appears to indicate that the behavior of the model over the observed population ranges in 1986-2008 is quite similar for very different values of the parameters.

Table 2.2: Observed parameter ranges for 50 runs of parameters fitted to oyster and black drum system in (2.20). See Figure 2.13 to see the similarity that these different parameters show in their forward orbits.

parameter	*min*	*max*
a	0.03	8.31
b	0.13	33.63
d	5E-3	0.74
h	2E-3	0.29
k	2E-5	0.08
c	0.50	113.60
m	1.43	3.19
r	0.53	1.67

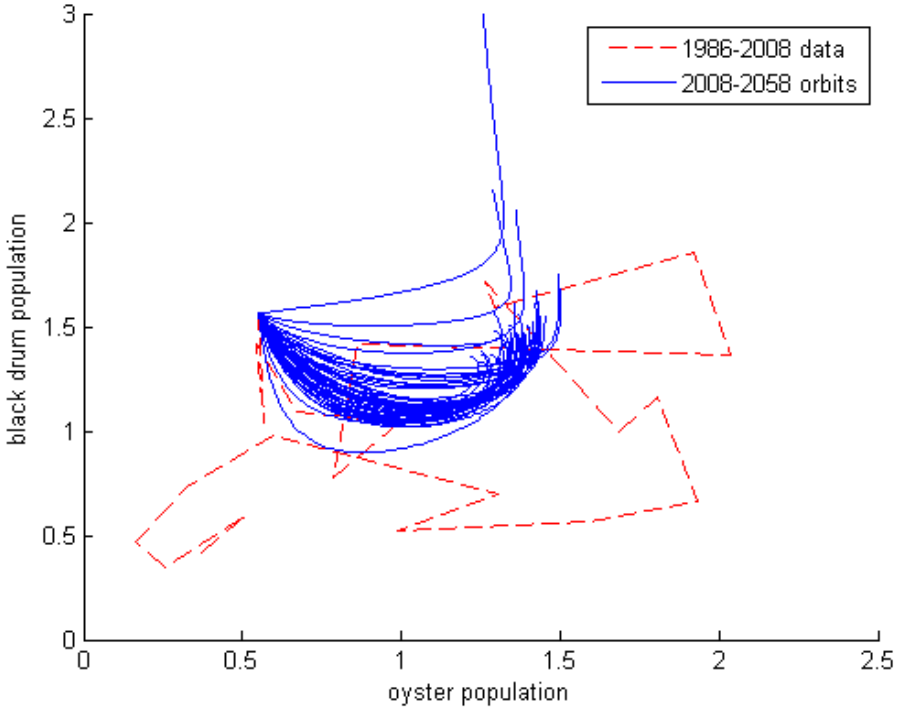

Figure 2.13: Population data for the period 1986-2008 and forward orbits of (2.19) for 50 years (2008-2058) using 50 different sets of parameters derived from our optimization routine. One run goes off the top of the figure and by year 50 reaches a black drum population of 3.45.

The observed range of parameters after treatment by the minimization scheme is shown in Table 2.2. All parameters show a large range of values, and most parameters show a range of more than an order of magnitude. The 1986-2008 population data and the forward time projections for 50 years (2008-2058) of all 50 runs are shown in Figure 2.13. The forward time evolutions began from the 2008 population data and used the average harvest over 1986-2008 as the harvest rate. One run goes off the top of the figure and by year 50 reaches a black drum population of 3.45. Two other runs show relative high final black drum population around 2. All others have a similar black drum population roughly near 1.5 and an oyster population between 1.2 and 1.5.

The population data show a large variation from year to year, a behavior not seen in the forward time orbits modeled by (2.20). This level of noise does not fit the data that can be predicted by the model. Based on [22], at least for the black drum, this noise is mostly observation error, rather than noise in the actual population over the period.

The value of the objective function for each run was quite similar, varying from 2.22 to 2.28. This is quite close to the minimum value that we have seen in any context, 2.21, which we found exploring the system using the optimizer "snopt" in the mathematical programming language AMPL [27] at the highly unrealistic choice of parameters $a = 39,606.3, b = 106.72, d = 0.22, h = 0.08, k = 0, c = 466.71, M = 165.89, r = 85.39$. Despite being clearly unrealistic, especially in terms of the growth rate, r, the forward orbit using these parameters is similar to the 50 orbits in Figure 2.13, consistent with our indications that different looking parameters can lead to similar values of our objective function and similar population predictions over several decades.

2.8 Conclusions

We found that the ratio-dependent predator-prey model with constant harvests, (2.4), can exhibit rich dynamical behavior, including the Takens-Bogdanov bifurcation. Depending on the parameter values, universal extinction, a single attractor, or multiple attractors are possible for the model. A global attractor other than extinction is only possible in the

absence of any harvest. Otherwise, there is always some initial condition where at least one of the harvests is too large for the initial population.

Limit cycles exist for the model with both harvests nonnegative, as had been found in the earlier papers ([57, 55, 56]) that considered the special cases, but we found numerical indications that stable limit cycles are a lot less persistent when the prey harvest is at least 0.03 than in the case without a prey harvest. Further investigation of the region of persistent limit cycles is proposed.

We also found that under (2.4) the predators may be saved from extinction by an increase in their harvest. This may be counterintuitive to some, but is consistent with the sense that many wildlife managers have that culling a population can be good for its future health.

Finally, we apply (2.4) to the oyster and black drum system on the public oyster grounds in Louisiana. Our numerical indications are that widely different choices for the parameter values can fit the data near optimally and produce similar forward projections under the model. It would be interesting to compare these predictions under (2.4) to predictions under other predator-prey models, to see if those results would be similar. If disparate models also act similarly over the observed range of data, that would explain some of the failure of consensus in the modeling community. It would also argue against extrapolation beyond the range of observed data under any particular model. We also propose comparison of our results to those of the more complex modeling software Atlantis.

Chapter 3: Single-species difference equation model

In this chapter, we consider a single-species difference equation model:

$$x \mapsto x + rx(1-x) - mx^c, \tag{3.1}$$

with $r, m > 0$ and $c > 1$. This model is an adaptation of the discrete logistic model for biological population growth

$$x \mapsto x + rx(1-x). \tag{3.2}$$

In this case, we have subtracted a variable human harvest mx^c from (3.2) to obtain (3.1), which we will motivate more below, but which roughly represents a resource user or manager who reacts to a declining population by decreasing the harvest. We developed the model (3.1) ourselves, and to our knowledge, it has not been previously seen or analyzed in the literature.

3.1 Background

Recall from the introduction that standard economic models predict over-exploitation in a fishery. Typically, this is used to argue for centralization of control. To avoid the sunken costs associated with open access and for general ecological health, fishery managers set a total allowable catch. However, centralization may also act against the future health of the resource. Behavioral research has shown that respect for regulations of a common pool resource declines when the decision makers are more distant from the resource users [46].

With this in mind, we consider an agent model where actors are incentivized to care about the future value of the resource stock. In this model, agents would purchase quota for multiple seasons: as modeled here, the right does not expire at all, but they could then

sell the rights back in the future for some fraction of the original cost. The remaining rights for this stock would only be re-sold under conditions described below. In this way, when a stock becomes depleted, agents would be incentivized to sell their rights and discontinue fishing, which would reduce the pressure on the fish stock. In other words, the fishery would be stabilized, since agents would respond to their perception of a poor future for a stock by allowing the stock to recover.

For our initial test of this sort of regulation, we created a simple model of both fish and fisher dynamics. Building on the suggestion of Hilborn in [35], our purpose with the model is to capture all important behavior in the simplest framework possible, for tractability and comprehensibility, so that reasonable conclusions could be drawn from the model. With this choice, we are moving in the opposite direction of Atlantis and similar computer models.

Since most commercially harvested species actually have seasons where fishers can either participate or not, we choose a discrete model, specifically the model 3.2 as the simplest model that captures the major dynamics of a single population. For the harvest, we needed to model the agents' response to changes in resource population. Initially, we assume that agents do not completely drop out. Imagine a single agent that responds in some way to a declining population with a decline in harvest. We will use a discrete model where the time, t, is an integer. We seek a natural choice for a total harvest, $h(t)$, that varies over time in a manner related to $x(t)$. The harvest, $h(t)$, should change in the direction of the change in population $x(t)$. In other words, the harvest should decrease in response to a declining population and increase in response to a recovering population. I chose $h(t)$ to change by a factor that is a function of $x(t)/x(t-1)$. The simplest such function would be to let $h(t)$ actually equal $h(t-1)x(t)/x(t-1)$, but this would keep the proportion harvested constant over time. In a classic modeling assumption (for example, in [8]), yield is proportional to effort times population. With this assumption and $h(t) = h(t-1)x(t)/x(t-1)$, effort would remain constant regardless of return, which is not anticipated in most economic models. It seems reasonable, then, that a harvester or manager might respond to a continually declining population by decreasing the proportion harvested. I model this with $h(t) =$

$h(t-1)(x(t)/x(t-1))^c$ with $c > 1$. To my knowledge, this choice of $h(t)$ has not been previously studied, although it is arguably the simplest function that satisfies the desired modeling properties. Subtracting this harvest from (3.2), we obtain:

$$x(t+1) = x(t) + rx(t)[1 - x(t)] - h(t)$$

$$h(t) = \left(\frac{x(t)}{x(t-1)}\right)^c h(t-1)$$

which, letting $m = h(0)/x(0)^c$, simplifies to become (3.1). Note that nothing prevents x from becoming negative in (3.1). I treat any negative population as extinct, consistent with the interpretation in the continuous models in [55] and [56].

Previous discrete models involving variable harvest are generally much more complicated. Many involve maximizing some form of explicit profit function [53, 7]. The model in [28] combines random search theory and the variable quota, Q, given by $Q \mapsto Qe^{a+bx-dQ}$ where a, b, d are constants and x is the population. However, our more tractable model captures the important dynamics of both the population and the harvesters and we use this model, so that the factors leading to its conclusions remain understandable.

3.2 Analytical Results

First, we analyze the dynamics of (3.1).

Theorem 6. *The map* (3.1) *has 2 fixed points:* 0 *and a unique strictly positive fixed point.*

Proof. Let $g(x) = rx(1-x)$, $h(x) = mx^c$. A value y is a fixed point of (3.1) if and only if $g(y) = h(y)$. Clearly, $g(0) = 0 = h(0)$, so 0 is a fixed point. To prove the existence of the unique, strictly positive fixed point, note first that $g'(0) = r$ and $h'(0) = 0$. Since $g'(0) > h'(0)$ and $g(0) = h(0)$, there exists a small $\epsilon > 0$ such that $g(\epsilon) > h(\epsilon)$. Now, $g(1) = 0$ and $h(1) = m$. Since $g(1) < h(1)$, there must be some $\tilde{x}$ between ϵ and 1 such that $g(\tilde{x}) = h(\tilde{x})$, giving us a strictly positive fixed point. To see that $\tilde{x}$ is unique, note that g is

concave and h is convex. $\square$

Note: The concavity arguments in the above proof also show that (3.1) belongs to a class of maps known as unimodal maps, whose mapping function has a single extremum.

We will use $\tilde{x}$ to denote the positive fixed point of (3.1) and let $f(x) = x+rx(1-x)-mx^c$. The fixed point of (3.1) at 0 is unstable since $f'(0) = 1 + r$ and $|1 + r| > 1$. Biologically, this means that extinction cannot occur by slow decline. Extinction, if it is possible, can only occur as an over-reaction to a high population.

We now turn our attention to the stability of $\tilde{x}$, which depends on our choice of c, m, and r. We have determined the region in c, m, r-space where this positive fixed point is stable (except for knowing stability on the boundary of the region). We first note that it is a basic calculation to show that for $c = 2$, $\tilde{x}$ is stable if $r < 2$ and unstable for $r > 2$. For all other values of $c > 1$, the stability is demonstrated in the following theorem:

Theorem 7. *Suppose $c < 2$. Let $q = (cr - r - 2)/(cr - 2r)$ and $B = \frac{r(1-q)}{q^{c-1}}$ for $q > 0$, ∞ for $q \leq 0$. Then the positive fixed point $\tilde{x}$ of (3.1) is:*

(i) stable if $m > B$

(ii) unstable if $m < B$.

The inequalities for these conditions reverse when $c > 2$.

Proof. $f'(x) = r - 2rx - cmx^{c-1} + 1$.

Since $\tilde{x}$ is a fixed point, $m\tilde{x}^c = r\tilde{x}(1 - \tilde{x})$. Dividing through by $\tilde{x}$, we have $m\tilde{x}^{c-1} = r(1 - \tilde{x}) = r - r\tilde{x}$.

Thus, $f'(\tilde{x}) = r - 2r\tilde{x} - c(r - r\tilde{x}) + 1$.

Let $j(y) = r - 2ry - c(r - ry) + 1$. Since $\tilde{x} \in (0, 1)$ and j is linear, $f'(\tilde{x})$ is between $j(0) = r - cr + 1$ and $j(1) = 1 - r$. Since $r > 0$ and $c > 1$, both $j(0)$ and $j(1)$ are less than 1, so $f'(\tilde{x}) < 1$ and stability occurs whenever $f'(\tilde{x}) > -1$. Simple calculation shows that $j(y) = -1 \iff y = q$. We now assume that $q > 0$ and return to our previously defined functions g and h. We know that $g(0) = h(0)$ and that $g(\tilde{x}) = h(\tilde{x})$. Thus, from the

fact that g is concave and h is convex, $g(x) < h(x)$ whenever $0 < x < \tilde{x}$ and $g(x) > h(x)$ whenever $x > \tilde{x}$. Specifically, $\tilde{x} < q \iff g(q) < h(q)$, for which basic calculation shows the condition is true if and only if $m > \frac{r(1-q)}{q^{c-1}}$. Similarly, $\tilde{x} > q \iff m < \frac{r(1-q)}{q^{c-1}}$. Clearly, when $q < 0, \tilde{x} > 0 > q$.

The slope $j'(y) = -2r + cr$, which is negative for $c < 2$. Thus, for $c < 2$, combining with the above analysis, $j(\tilde{x}) > -1$ if $m > B$ and $j(\tilde{x}) < -1$ if $m < B$. When $c > 2$, the slope of j reverses and $j(\tilde{x}) > -1$ if $m < B$ and $j(\tilde{x}) < -1$ if $m > B$. □

3.3 Numerical Results

There are also many numerical indications for (3.1). Based on trial runs, it appears that asymptotic behavior of (3.1) can be a steady state, a periodic orbit, chaos or extinction, only depending on the choice of c, m, and r as long as the initial population, $x(0)$, is positive and does not immediately lead to extinction. ($f(x(0)) > 0$.) Results for some choices of different parameter values are shown in Figure 3.1, and a bifurcation diagram with m varying and $r = 0.08, c = 100$ is shown in Figure 3.2. The value $r = 0.08$ was chosen for all our implementations of this model since it is the growth rate the National Marine Fisheries Service uses to model fur seals [45]. As a marine mammal estimate, 0.08 should provide low growth and, thus, be a conservative estimate for recovery in our simulations seen in later sections. The value $c = 100$ is used to show a value where chaos is evident. The c-value is not intended to be realistic. For each value of m in the diagram, we ran for 1,000 transient iterates and plotted the next 1,000 iterates, which appeared sufficient to show the bifurcations of the model.

3.4 Agent-based models using the single species equation

There are multiple adaptations to the single-species equation (3.1) that can be made. One such adaptation is to have heterogeneous agents. Suppose there are N harvesters of the

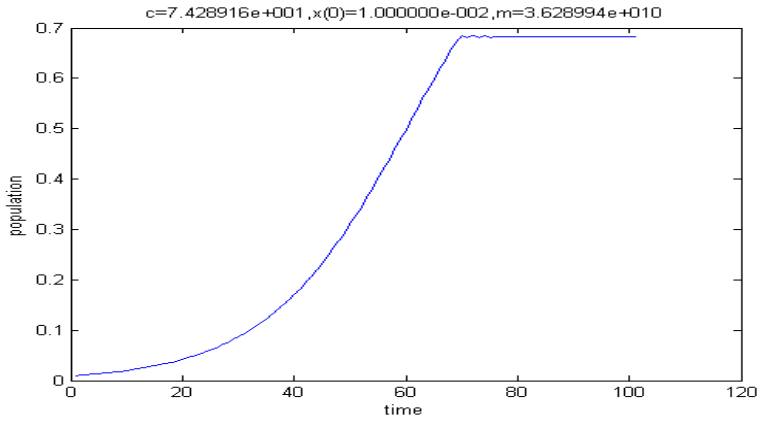

(a) Population over time for the single species equation (3.1) with a $r = 0.08$ and a stable fixed point

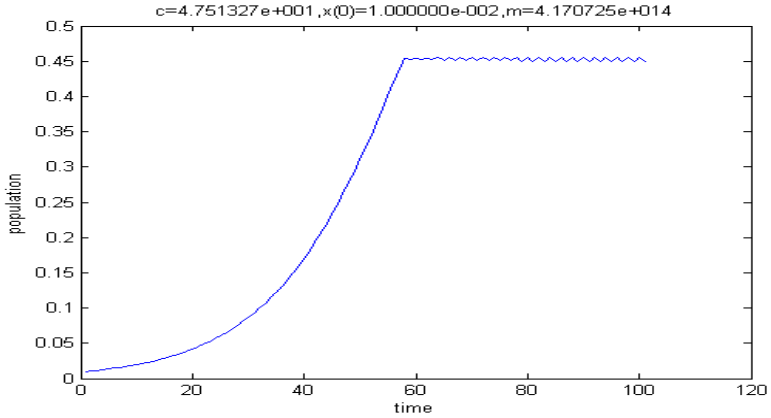

(b) Population over time for the single species equation (3.1) with $r = 0.08$ and without a stable fixed point

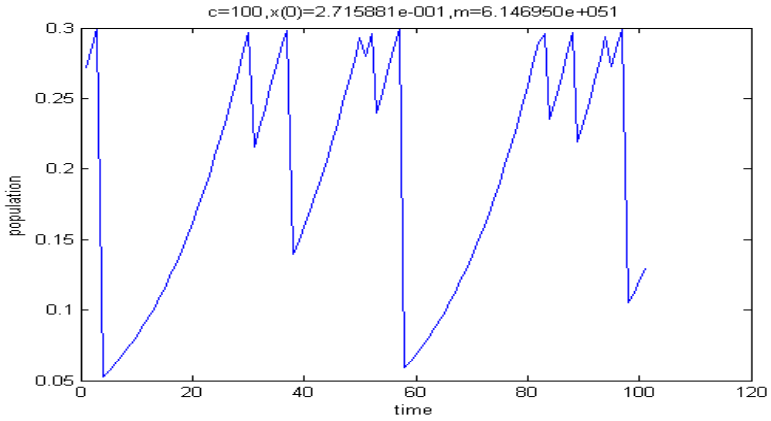

(c) Population over time for the single species model (3.1) with $r = 0.08$ and parameters chosen that appear numerically to result in a chaotic orbit

Figure 3.1: The population over time for model (3.1) with the parameter choices indicated. In 3.1a, the population becomes fixed asymptotically. In 3.1b, the population tends to a 2-cycle. In 3.1c, the dynamics appear chaotic.

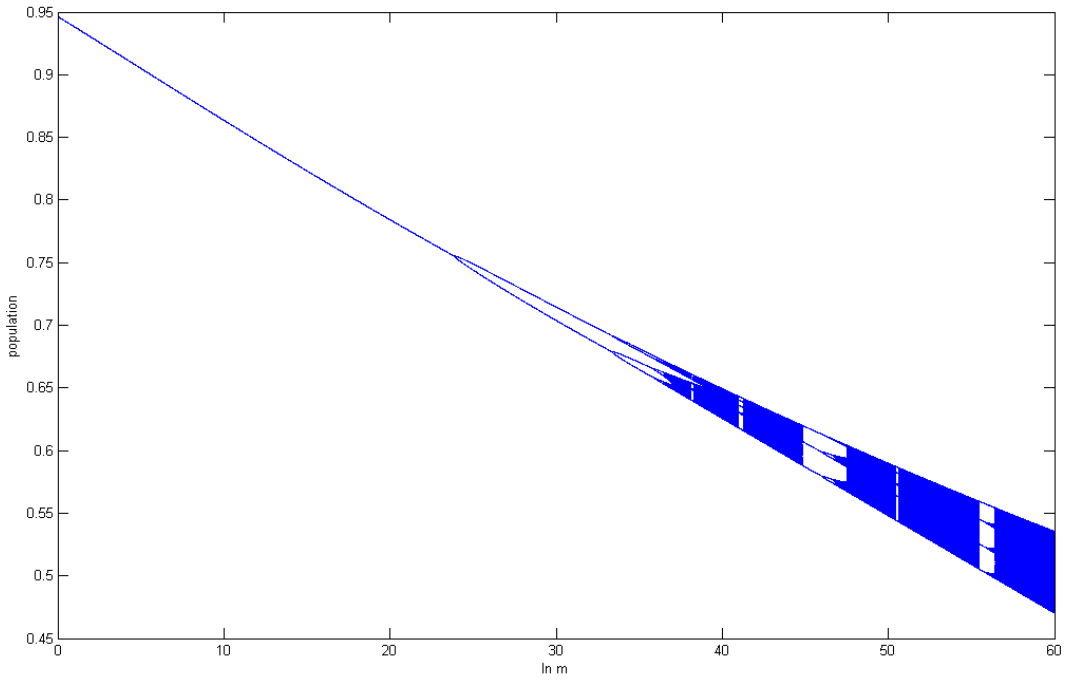

Figure 3.2: Bifurcation diagram of the model (3.1) with $r = 0.08$ and $c = 100$. The plot shows the 1,000 iterates after 1,000 transient iterates for each m-value.

same resource, each harvesting as in (3.1), but each with a different m and c, that is

$$x \mapsto x + rx(1-x) - \sum_{i=1}^{N} m_i x^{c_i} \tag{3.3}$$

The agent model, by its structure, inherits similar properties to (3.1): an unstable fixed point at 0, unimodality, and a unique positive fixed point.

For any given year, we will use the notation $h(t) = \sum_{i=1}^{N} m_i x^{c_i}$. In a multi-year simulation, we will use the notation H for the total harvest, that is $H = \sum_{t=0}^{M} h(t)$, where M is final year of the simulation. We use the relatively slow growth rate of $r = 0.08$ for all the following runs.

3.4.1 Stability

The region of stability for (3.3) is not clear analytically, so we analyze the agent model numerically. In particular, we ask: if the positive fixed point were to be stable for some harvesters acting alone, but not for others, how would it be overall? We create a simulation as follows. When $r = 0.08$, it follows by simple calculation and Theorem 6 that the fixed point must be stable when $c < 26$, and may be stable or unstable (depending on m) when $c > 26$. For each agent, we determine a c_i by dividing 26 by a random number chosen by MATLAB from a uniform distribution between 0 and 1. By Theorem 6, this c_i determines a bound B_i for m above which the fixed point would be stable if the agent were acting alone. We choose another random number (say a_1) from a uniform distribution between 0 and 1, and we let $m_i = B_i/a_i$ if we want the agent to be stable and $m_i = B_i a_i$ if we want the agent to be unstable. In this way, we can determine the stability if the harvester acted alone. We conducted an experiment with 50 stable agents and 50 unstable agents.

As seen in Figure 3.3, we observe intermediate behavior in the agents in terms of dynamics: somewhere heuristically less stable than a single agent whose behavior leads to a stable equilibrium and a single agent whose behavior leads to an unstable equilibrium. In fact, it

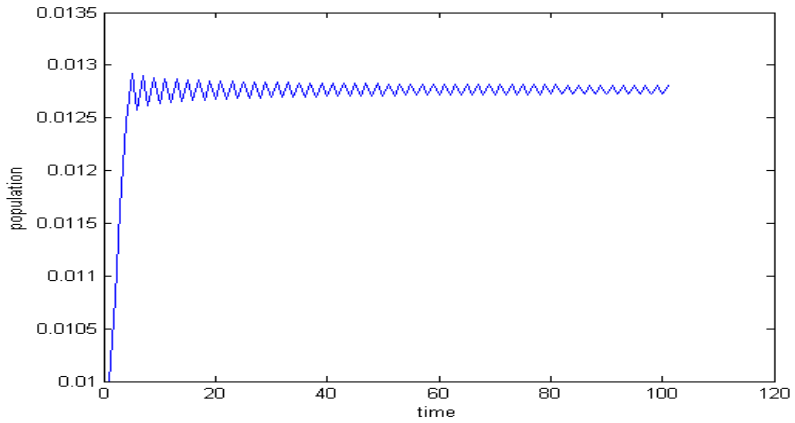

Figure 3.3: Population over time for the agent model (3.3) with 100 agents where the fixed point would be stable for half of the agents acting alone and unstable for the other half of the agents acting alone. The harvested species' growth rate, r, is 0.08 and the harvest parameters for each agent were chosen randomly as we described. The dynamics are intermediate with respect to stability of the positive fixed point. In fact, even by t=1,000 (not pictured in the figure), the population neither settles on a 2-cycle nor a fixed point.

is unclear in simulations whether the fixed point is stable. By several lifetimes ($t = 1,000$), the population has still not settled on a fixed point, but the width of the oscillations is still decreasing. The asymptotic population value of the agent model is much smaller than that for (3.1), which would be expected, since there are 100 times more harvesters.

3.4.2 Runs of (3.3) starting from $x(0) = 0.75$ and $h(0) = 0.09$

We first consider the starting point with a single agent, i.e. using (3.1). For this simulation, we chose an initial population (0.75) between the unharvested equilibrium ($x = 1$) and the maximum sustained yield population ($x = 0.5$) to represent a population in the early stages of harvest. We also the initial harvest, $h(0)$, is unsustainable. The maximum growth rate achieved by the model is 0.02, so it will not be possible to continue to harvest at that rate. In fact, the proportion initially harvested, 0.12, was also chosen to be unsustainable. If the proportion harvested is constant, then $c = 1$, and with our initial harvest, $h(x) = 0.12x$, the only fixed point for our model is a stable fixed point at 0 ($f'(0) = -0.04$). The population

will be driven to 0 for a single agent with $c = 1$. These values were chosen to allow extinction by slow decline in these two cases.

For $c > 1$, extinction is only possible when $f(f_{max}) \leq 0$ where f_{max} is the maximum value obtained by f. For these initial assumptions, numerical calculation shows $f(f_{max}) \leq 0$ only for unrealistically large values of c ($c > 334$). For the values of c that we consider, the population will drift towards a stable fixed point. We chose 1,000 year simulations, since that length is enough to see the asymptotic behavior of the model, if it can recover from the initial overfished condition. Numerical indications show that for 1,000 year simulations, H is maximized at about 20.24 when c is about 3.7 (which implies $m = 0.2609$).

In all our multi-agent runs, when we create heterogeneity among the agents, we will do so using an even distribution in all dimensions where the agents differ. For the initial harvest, we divide a chosen initial harvest among the agents as follows: each agent is assigned a random number from a uniform distribution on [0,1]. The initial harvest is divided in proportion to these random numbers. We expand our range of c considered for the model to include the limiting case $c = 1$, modeling agents whose fishing effort is entirely unresponsive to payoff. As seen above, when $c = 1$ for a single agent, extinction is expected for our initial conditions since the fixed point at 0 becomes stable. For that reason, we label these agents as "extinction" harvesters. The agents are then divided in two categories: "extinction" harvesters (with $c_i = 1$), and "efficient" harvesters (with c_is for efficient harvesters chosen by MATLAB from a uniform random distribution on [1,6.4]). "Efficient" harvesters are given that name since the most efficient c value, 3.7, is the midpoint of the interval [1,6.4]. Individually, the members of this group may not be acting efficiently, but, in some sense, the average harvester is efficient. Calculation of $f'(0)$ shows that the fixed point may or may not be stable for this agent model depending on how much of the initial harvest was owned by extinction harvesters. The dynamics continue to show a drift towards a single fixed point, the value of which decreases with the number of extinction harvesters, reaching 0 when all the harvesters are extinction harvesters. The values of H for 1,000 year simulations with 100 agents are shown in Table 3.1. We chose 100 agents since it is roughly (order of

Table 3.1: Total harvest (H) by proportion of harvester agents (E) who have $c_i > 1$ for runs starting from $x = 0.75$ and $h = 0.09$. The case where $c_i = 1$ corresponds to constant effort.

E	H
100%	20.16
90%	19.98
80%	19.52
70%	18.61
60%	15.30
50%	11.19
40%	6.36
30%	2.44
20%	1.62
10%	1.54
0%	1.36

magnitude) correct for many fisheries.

From the first line of the table, we see that 100 agents with c_i's chosen randomly from [1,6.4] gives a very similar result to a single agent with $c = 3.7$. We also see that efficiency is fairly robust to even a sizeable minority of extinction harvesters, but begins to drop off noticeably after about 30 extinction harvesters. We also see that inefficiency is robust to a similar minority of efficient harvesters.

It may seem unusual from typical price theory, but a study of cab drivers in [11] found that a simple heuristic of a constant income per day may result in more effort when profit is lower. Using a similar heuristic of a constant harvest no matter what the effort required, we now repeat this using a different definition of extinction harvesters ($c_i = 0$) and efficient harvesters (c_i chosen from a uniform distribution on [0,7.4]). The results are shown in Table 3.2. In this case, efficiency is not robust to a minority of extinction harvesters, but does continue to be robust to c_i's chosen from [0,7.4], rather than actually 3.7.

Table 3.2: Total harvest (H) by proportion of harvester agents (E) who have $c_i > 0$ for runs starting from $x = 0.75$ and $h = 0.09$. The case where $c_i = 0$ corresponds to constant harvest.

E	H
100%	20.14
90%	2.68
80%	1.41
70%	1.17
60%	1.04
50%	1.01
40%	0.99
30%	0.95
20%	0.94
10%	0.93
0%	0.91

3.4.3 Runs of the agent model with $x(0)$ varying

Here, we vary $x(0)$, and, to retain the value of 3.7 as the most efficient c in long-term simulations, we tie the initial harvest, $h(0)$, to $x(0)$ by the formula $h(0) = 0.2609x(0)^{3.7}$. This formula keeps the location of the fixed point at the maximum sustained yield value of $x = 0.5$. It also means that the initial harvest remains unsustainable as long as $x(0) > 0.5$. We seek to determine whether starting closer to a sustainable harvest will allow efficiency to remain in the presence of a sizeable minority of extinction harvesters. In this section, we use the definition of extinction harvesters as $c_i = 0$ and efficient harvesters as c_i chosen from a uniform distribution on [0,7.4], as before, still centered on the most efficient values. Call the proportion of efficient harvesters (out of 100 total harvesters) E. We ran 1,000 year simulations with E varying from 0.01 to 1. As the population of the harvested species declines, efficient harvesters lower their harvest and extinction harvesters do not, so it not surprising that the runs that avoid extinction are the runs with the highest E. This is typically, but not always, observed. The results are shown in Table 3.3. Since on that time scale, extinction was quite common for all initial conditions, we also ran our simulations on

Table 3.3: Percent (p) of runs that avoid extinction in 1,000 year simulations by initial population ($x(0)$) using $c_i = 0$. 100 runs were performed with E varying from 0.01 to 1.

$x(0)$	p
1.00	0%
0.95	0%
0.90	0%
0.85	1%
0.80	4%
0.75	5%
0.70	9%
0.65	17%
0.60	29%
0.55	49%

the more foreseeable time scale of 100 years. Results for 100 year runs are shown in Table 3.4.

In the 1,000 year time window, the majority of runs went extinct even when starting at $x(0) = 0.55$, near the maximum sustained yield population of 0.5. So, in the end, this system is sensitive to a combination of initial harvests that are too high and/or a minority of fishers that continue with a constant harvest as the population declines.

3.4.4 Runs with a stochastic fish population, $x(0) = 0.5, h(0) = r/4$.

These runs start with harvest and population at the theoretical maximum sustained yield (MSY) value, which is a fixed point for the deterministic system. All agents have the same c (which is mathematically equivalent to having a single agent). Note that the MSY equilibrium is stable for $0 < c < 50$ (when $r = 0.08$). In the 100 year runs shown in Table 3.5, we added a random number from a normal distribution with mean 0 and standard deviation 0.05 is added to the population each year. We chose the standard deviation of 0.05 rather arbitrarily. In future work, we propose repeating these experiments with a standard deviation derived from population data. Because any stochasticity makes extinction in the long term likely, we chose the foreseeable time scale of 100 years. In each run, c was fixed

Table 3.4: Percent (p) of runs that avoid extinction in 100 year simulations by initial population ($x(0)$) using $c_i = 0$. 100 runs were performed with E varying from 0.01 to 1.

$x(0)$	p
1.00	1%
0.95	0%
0.90	0%
0.85	3%
0.80	6%
0.75	11%
0.70	17%
0.65	27%
0.60	38%
0.55	65%

for the run. From each run, H and x_{min} (the minimum value attained by x over the run) were recorded. There was variation over the runs due to stochasticity. Thus, we performed 1,000 runs for each value of c, and the median values for H and x_{min} are recorded in the table. We chose 1,000 runs because we could run all our experiments of this type within several hours of computing time with that value. For a deterministic model, beginning at a fixed point would mean the population and harvest would remain constant over time, and H for the deterministic model would be $100h(0) = 200$ and x_{min} would be $x(0) = 0.5$ for any choice of c. We find that, for $c \geq 1$, similar values of the total harvest are obtained for the simulation as would be seen in a deterministic model.

3.5 Drop-outs and New Fishers

We now make two adjustments to all of the models in the previous subsection, and run the results again. The first is that agents have a threshold population, and when the population drops below that threshold, the agents drop out permanently from harvesting. This is consistent with the possibility of selling back the right to fish as discussed in Section 3.1, and a further assumption that the price of fish does not increase enough as the fish become

Table 3.5: Total harvest (H) and minimum population (x_{min}) by c

c	H	x_{min}
0	1.83	0
1	1.98	0.20
2	2.00	0.23
3	1.99	0.25
4	1.99	0.25
5	2.00	0.27
6	2.04	0.27
7	2.01	0.27
8	1.99	0.27
9	1.97	0.27
10	1.99	0.27
11	1.99	0.27

rare to offset the increased effort. This assumption would be satisfied, for example, by the modeling of price as constant (such as in [8]) for a species where replacements are available in the market. Each agent has a threshold chosen from a uniform distribution between 0 and $x(0)$ below which they will stop fishing (and not return). This prevents extinction in the vast majority of agent runs without a stochastic element, and makes extinction less likely in runs with a stochastic element. However, it does not return efficiency to the model since once fishers drop out, they do not re-enter, even when the population rebounds, so another addition to the model was introduced. New fishing rights are created and sold to new agents. These new agents have a c chosen in the same way as the initial population, but the threshold population for the new agents is on a uniform distribution between 0 and the population at the time of their re-entry, rather than between 0 and $x(0)$. A rule that was found to balance efficiency and extinction concerns was used to determine when new fishing rights were sold. If for 3 consecutive years, the increase in population was greater than the harvest, then 40% of the minimum population increase over the 3-year period would be sold to new fishers, with the division of the new fishing rights done in the same stochastic way as the division among the original fishers. The number of years and percentage in

this rule were found to work, in practice, for our rather arbitrary choice of stochasticity of 0.05. When we have stochasticity available from real-world data set(s), we propose further analysis of the effect of these two numbers on performance of the rule. The number of new fishers would be equal to the number of current fishers, up to a maximum of 5,000 fishers, the most fishers we could plausibly imagine in a fishery. We will refer to this method in the sections below as "drop-outs and new fishers".

3.5.1 Runs of (3.3) with drop-outs and new fishers starting from $x(0) = 0.75$ and $h(0) = 0.09$

We conduct a similar experiment as in 3.4.2, with drop-outs and new fishers. As before, the agents are then divided in two categories: "extinction" harvesters (with $c_i = 1$), and "efficient" harvesters (with c_i's chosen from a uniform random distribution on [1,6.4]). We retain the name efficient harvesters even though the midpoint 3.7 is no longer expected to maximize H. The agents who drop out and the unknown population where new agents might be added make the calculation of the most efficient c less trivial, but 3.7 gives results in the ballpark of the optimal H. The logical maximum H for this scenario, based on standard MSY analysis as in [15] is 20.25. The dynamics again show a drift towards a single fixed point, but the value of the fixed point varies much more noticeably due to the random elements. For that reason, we conduct 100 runs and report median values for each proportion of harvester agents. The values of H for 1,000 year simulations with 100 agents are shown in Table 3.6. Total harvest in all cases is shown in Figure 3.4. Note that the fishery is pretty efficient for all choices of E, even in the case where all fishers have constant effort ($E = 0\%$).

We repeated this experiment using the constant harvest definition of extinction harvesters ($c_i = 0$) and efficient harvesters (c_i's chosen from a uniform distribution on [0,7.4]). The results are shown in Table 3.7. Efficiency remains relatively strong, even when efficient harvesters become a minority, less so than when $c_i \geq 1$, but much more so than with constant harvest agents and no drop-outs or new fishers. See Figure 3.4 for a comparison

Table 3.6: Median total harvest (H) by proportion of harvester agents (E) who have $c_i > 1$ for runs starting from $x = 0.75$ and $h = 0.09$ for the model with drop-outs and new fishers.

E	H
100%	20.15
90%	20.21
80%	20.23
70%	20.22
60%	20.15
50%	19.97
40%	19.77
30%	19.53
20%	19.11
10%	18.75
0%	18.21

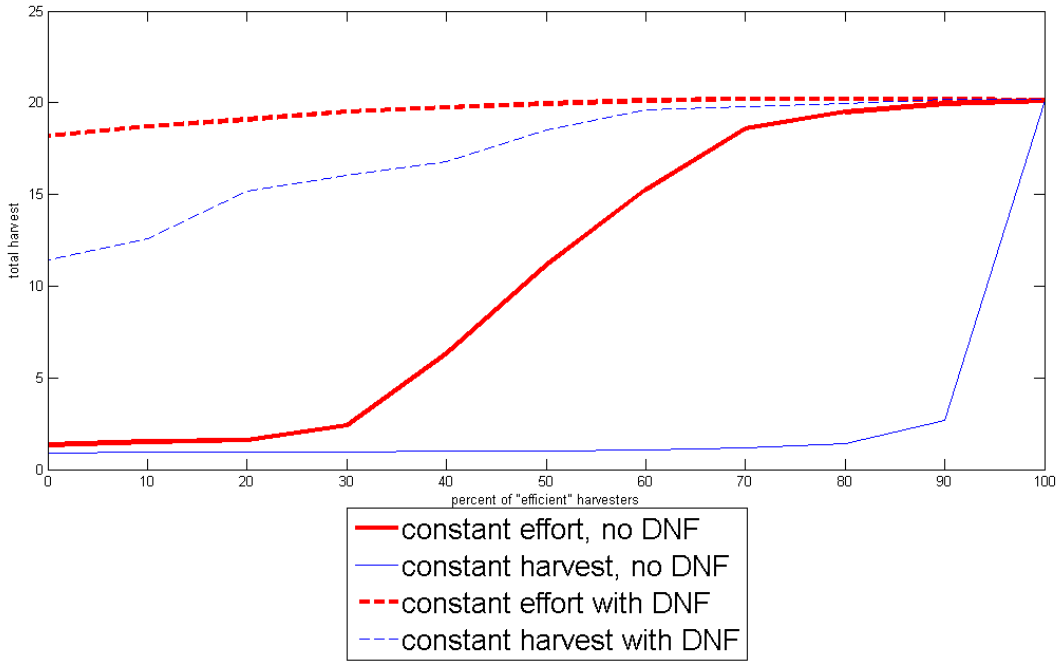

Figure 3.4: Total harvest for the agent model by percent of efficient harvesters with and without drop-outs and new fishers (DNF) and with both the constant effort and constant harvest definition of extinction harvesters.

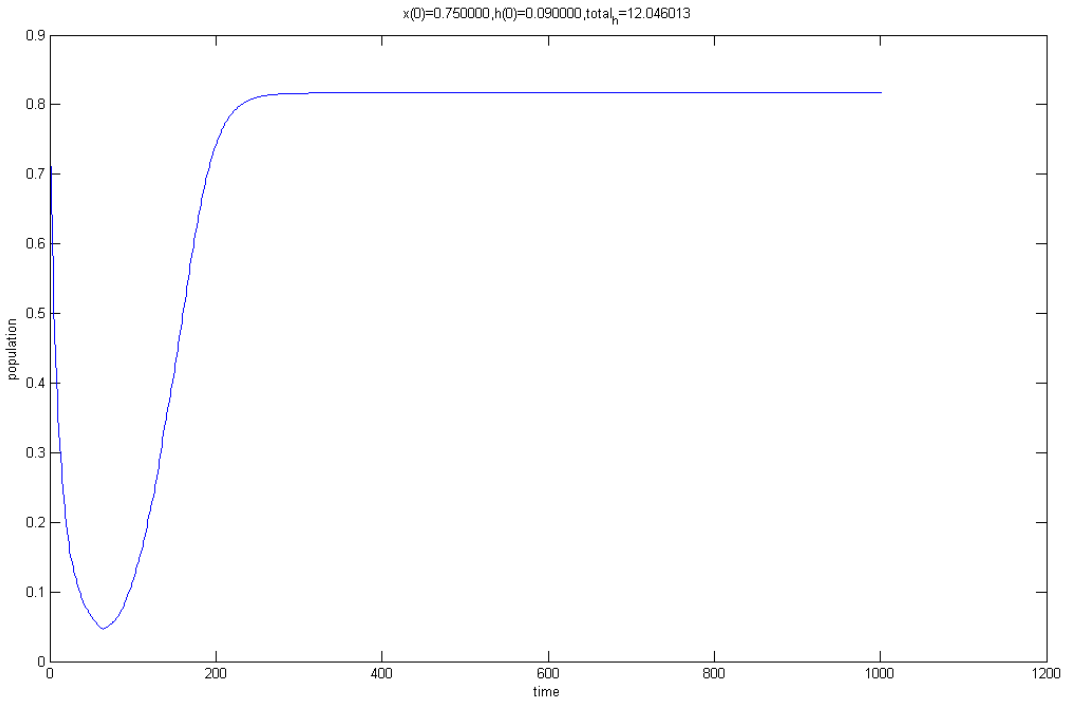

Figure 3.5: Population of the target species with drop outs and new fishers using an agent model where all fishers continue a constant harvest until they drop out, and the initial sum total of the agents is 4.5 times too high for MSY stability. The model shows a several-decade long crash, followed by a similarly slow recovery. It is likely that modeling some drop-outs due to retirement would limit the length of the crash and the resulting recovery.

Table 3.7: Total harvest (H) by proportion of harvester agents (E) who have $c_i > 0$ for runs starting from $x = 0.75$ and $h = 0.09$ for the model with drop-outs and new fishers.

E	H
100%	20.21
90%	20.20
80%	19.96
70%	19.77
60%	19.62
50%	18.51
40%	16.78
30%	16.05
20%	15.19
10%	12.59
0%	11.43

of these modeling assumptions. We also note that when the number of efficient harvesters is low, the fish population crashes and recovers before stabilizing, and that this process usually takes a long period: more than 100 years. (See Figure 3.5.) We anticipate that, in reality, this process of recovery would occur more quickly, since drop outs due to retirement would occur and quicken the time scale of recovery.

3.5.2 Runs of the agent model with $x(0)$ varying with drop-outs and new fishers

We now repeat the simulations from Section 3.4.3 with drop-outs and new fishers. We assume 100 agents and let $c = 0$ for all agents. Again, we vary $x(0)$ and find an $h(0)$ that in the single-agent case gives $m = 0.2609$ when $c = 3.7$). As seen in Tables 3.8 and 3.9, extinction is now rare.

Figure 3.6 shows a comparison to the similar simulation without drop-outs and new fishers. In the end, the drop outs and new fishers model allows the species to survive in the simulation.

Table 3.8: Percent (p) of runs that avoid extinction in 1,000 year simulations by initial population ($x(0)$) using $c_i = 0$ with drop-outs and new fishers. 100 runs were performed with E varying from 0.01 to 1.

$x(0)$	p
1.00	100%
0.95	98%
0.90	100%
0.85	100%
0.80	99%
0.75	100%
0.70	98%
0.65	100%
0.60	97%
0.55	99%

Table 3.9: Percent (p) of runs that avoid extinction in 100 year simulations by initial population ($x(0)$) using $c_i = 0$ with drop-outs and new fishers. 100 runs were performed with E varying from 0.01 to 1.

$x(0)$	p
1.00	100%
0.95	100%
0.90	99%
0.85	100%
0.80	100%
0.75	100%
0.70	99%
0.65	99%
0.60	98%
0.55	99%

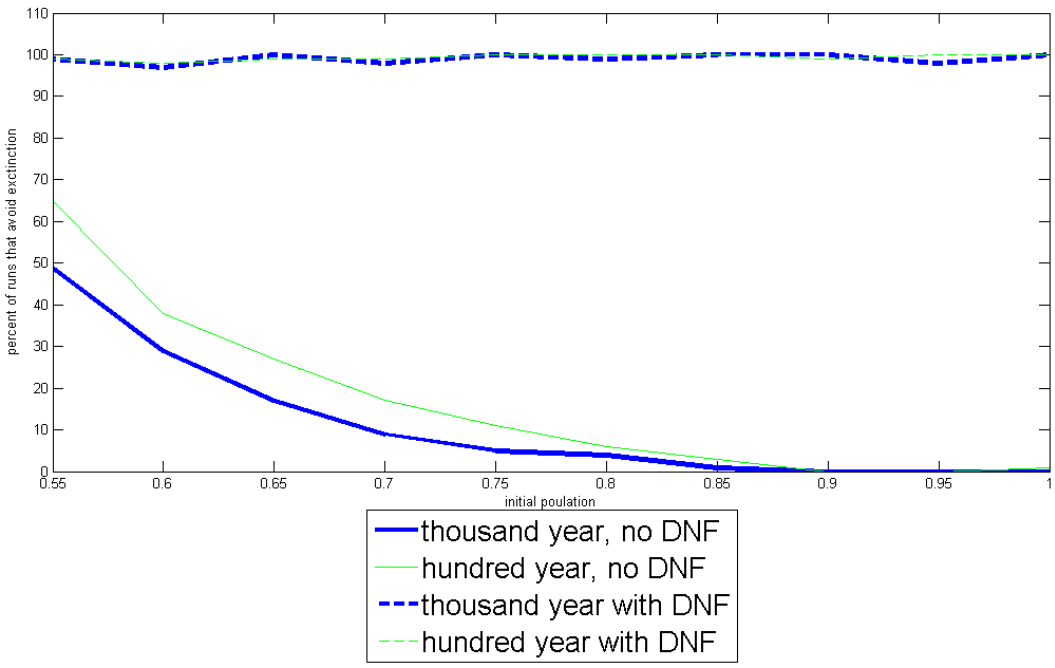

Figure 3.6: Percent of runs that avoid extinction for the agent model by initial population when initial population is tied to initial harvest. Results are shown with and without drop-outs and new fishers (DNF) and for 100 and 1,000 year simulations.

Table 3.10: Total harvest (H) and minimum population (x_{min}) by c with drop-outs and new fishers

c	H	x_{min}
0	1.83	0.01
1	1.98	0.15
2	2.00	0.19
3	1.99	0.21
4	1.99	0.24
5	2.00	0.24
6	2.04	0.25
7	2.01	0.25
8	1.99	0.25
9	1.97	0.24
10	1.99	0.23
11	1.99	0.23

3.5.3 Drop-outs and new fishers with a stochastic fish population, $x(0) = 0.5, h(0) = r/4$.

We repeat the stochastic runs using 100 agents with the same c. Median results for 1,000 runs are shown in Table 3.10. Comparisons of the minimum population seen and the total harvest are shown in Figures 3.7 and 3.8 respectively. We find that extinction is less likely in the $c = 0$ case, but otherwise the minimum population achieved is typically a little less with drop outs and new fishers. The total harvest, H, tends to be higher with drop outs and new fishers.

3.6 Conclusions

We have created a simple model 3.1 for initial evaluation of management tools. Leading fisheries scientist Ray Hilborn suggested in [35] that simple management rules can prevent some of the drawbacks of accuracy and access that have affected the more complex management tools in use today, in particular the lack of knowledge about the parameters of the

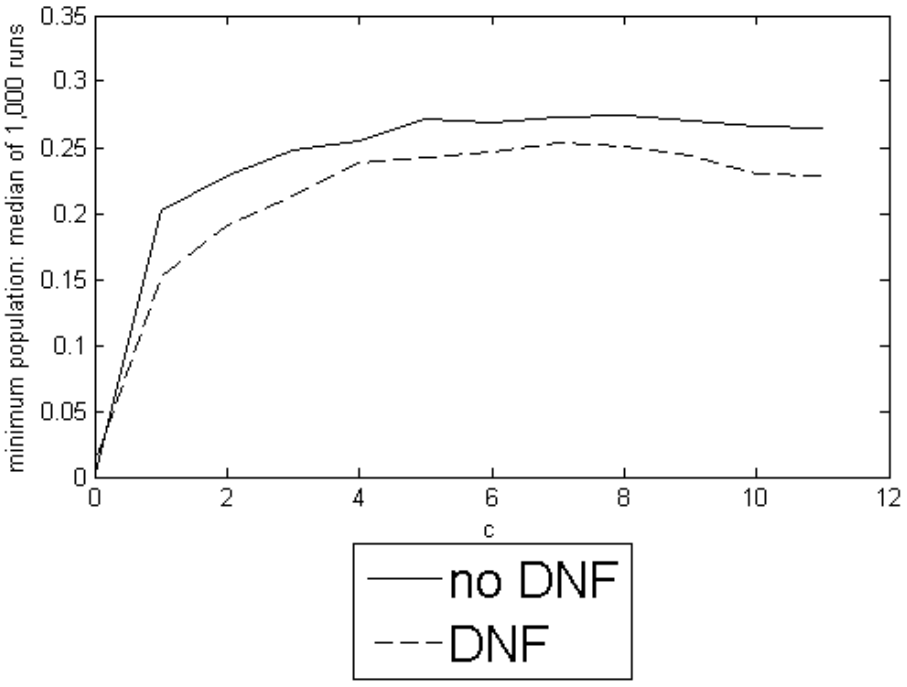

Figure 3.7: Minimum population seen during a 100 year simulation, for different values of c. Results shown are the median of 1,000 simulations.

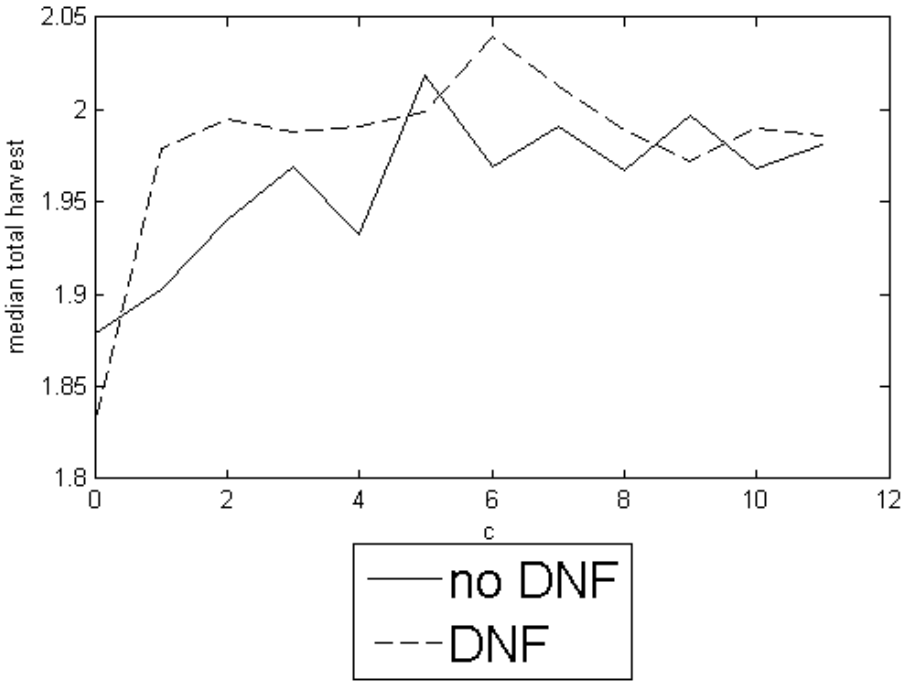

Figure 3.8: Total harvest for a 100 year simulation, for different values of c. Results shown are the median of 1,000 simulations.

model. We use 3.1 to test a simple management rule that assumes no knowledge of the underlying model on the part of managers, and find that this tool can return efficiency under some assumptions, particularly that of a proportion of harvesters who continue to fish the same amount or with the same effort as a population changes. We test efficiency against heterogeneity of agents, and find that the model retains efficiency against heterogeneous agents as long as the agents' behavior is centered on a correct value.

We tested further with harvesting classes that overfish initially and continue to fish with either constant effort or a constant harvest, and find that a sizeable minority of the former group and even a small minority in the latter group led to significant and economically inefficient overfishing. We found that fishers who drop out can prevent overfishing, but retain economic inefficiency since the resource becomes under-exploited over time. Thus, we demonstrated a simple management rule that returns efficiency in our hypothetical scenario.

The drop-outs and new fishers rule, in itself, has two dimensions on which it can be changed, the number of years of excess growth (in our case, 3 years) and the percent of excess growth that is sold back (in our case, 40%). These two parameters were found to work in our model, which has the rather arbitrary choice that stochastic element of the population should have a standard deviation of 0.05. In future work, we propose finding a reliable estimate of the standard deviation in one or more actual populations and finding the effect of changing these two dimensions.

While results suggest benefits to this rule, we present drop-outs and new fishers as a first step. We would like to see future work in the area of suggesting simple management rules under different assumptions. Work could also consider more complicated models as a verification of the robustness of the rule, as Hilborn also suggested in [35].

Chapter 4: Conclusions

We introduced these two different models of population levels of natural resource populations under harvesting with different emphases in mind in their application to commercial fisheries. For our first model, (2.4), the emphasis was on the dynamics of the underlying population of fish. For (3.1), the emphasis was more on the behavior of the fishers through its adaptation to the agent model (3.3).

We found that the dynamical structure of (2.4) included the Takens-Bogdanov bifurcation. We also found a wide variety of behavior in phase space, including universal extinction, a single attracting equilibrium, multiple attractors and, in a few cases, stable cyclical behavior. In addition, we found a pattern in the types of equilibria based on their prey populations, and that a predator harvest may actually prevent predator extinction in the long term.

We studied in particular the limit cycles of (2.4). We found that, especially with any positive harvest for both species, most stable limit cycles do not persist when the predator harvest changes.

In our application to the oyster and black drum populations in Louisiana, we found that the model predicts similar behavior for widely different parameter values. In fisheries management, this suggests that the model could be a useful tool over the observed range of population, but we would caution against its use to predict outside that range. We should also note that stochasticity is obviously present in the actual population.

Finally, we suggest further work in the area of model fitting. We remain interested to see whether entirely different models would show similar predictions for the oyster-black drum system that we applied (2.4) to. It would also be worthwhile to consider how this and other models fit other predator-prey systems, or even, using the same functional response, how the model behaves when applied to more than two species.

In Chapter 3, we modeled harvesting behavior. While previous work has either avoided modeling the harvest or focused on much more complicated ways of modeling it, we believe that our simple model has the advantage of having some tractability to analysis, but also models the important expected behavior of the model.

We were able to find a fairly simple rule that allowed agents, as a class, to behave near efficiency in the absence of any prior knowledge of what behavior would be most efficient. In this way, we contribute to a growing field of study along with [5], [54], and [8].

Bibliography

[1] Adams T (1998). The interface between traditional and modern methods of fishery management in the Pacific Islands. Ocean and Coastal Management 40:127-142.

[2] Akcakaya HR, Arditi R, and Ginzburg LR (1995). Ratio-dependent predation: An abstraction that works. Ecology 76: 995-1004.

[3] Andronov AA, Leontovich EA, Gordon II, and Maier AG (1971). Theory of Bifurcations of Dynamical Systems on a Plane.

[4] Arditi R and Ginzburg LR (1989). Coupling in predator-prey dynamics: Ratio-dependence. Journal of Theoretical Biology 139: 311-326.

[5] Arnason R (2009). Conflicting uses of marine resources: can ITQs promote an efficient solution? The Australian Journal of Agricultural and Resource Economics 53:145-174.

[6] Arnold A and Polking J (1999). Ordinary Differential Equations using MATLAB, Second Edition.

[7] BenDor T, Scheffran J, and Hannon B (2009). Ecological and economic sustainability in fishery management: A multi-agent model for understanding competition and cooperation. Ecological Economics 68: 1061-1073.

[8] Bischi GI, Lamantia F, and Radi D (2013). A prey-predator fishery model with endogenous switching of harvesting strategy. Applied Mathematics and Computation 219: 10123-10142

[9] Blanchet H (2010). Assessment of Black Drum in Louisiana Waters.

[10] Branch TA, Jensen OP, Ricard D, Ye Y, and Hilborn R (2011). Contrasting global trends in marine fishery status obtained from catches and from stock assessments. Conservation Biology 25: 777-786.

[11] Camerer C, Babcock L, Loewenstein G, and Thaler R (2000). Labor supply of New York City cab drivers: One day at a time. Choices, Values, and Frames (Kahneman D and Tversky A- eds.): 356-370.

[12] Castillo D and Saysel AK (2005). Simulation of common pool resource field experiments: a behavioral model of collective action. Ecological Economics 55: 420-436.

[13] Chu C (2009). Thirty years later: the global growth of ITQs and their influence on stock status in marine fisheries. Fish and Fisheries 10:217-230.

[14] Clark CW (1973). The Economics of Overexploitation. Science 181:630-34.

[15] Clark CW (2010). Mathematical Bioeconomics: The Mathematics of Conservation, Third Edition.

[16] Clark CW, Munro G, and Sumaila UR (2010). Limits to the privatization of fishery resources. Land Economics 86:209-218.

[17] Clark CW, Munro G, and Sumaila UR (2010). Limits to the privatization of fishery resources: response. Land Economics 86:614-618.

[18] Clerc M and Kennedy J (2002). The particle swarm: Exploration, stability, and convergence in a multi-dimensional complex space. IEEE Transactions on Evolutionary Computation 6:58-73.

[19] Costello C, Gaines, SD and Lynham J(2008). Can catch shares prevent fisheries collapse? Science 321:1678-1681.

[20] Cross R, Grinfeld M, Lamba H, and Seaman T (2005). A threshold model of investor psychology. Physica A 354:463-478.

[21] DeMutsert K, Cowan JH Jr., Essington TE, and Hilborn R (2008). Reanalyses of Gulf of Mexico fisheries data: landings can be misleading in assessments of fisheries and fisheries ecosystems. Proceedings of the National Academy of Sciences 105: 2740-2744.

[22] DeMutsert, Kim. Personal communication.

[23] Dong L (2008). A self-adapting herding model: The agent judge-abilities influence the dynamic behaviors. Physica A 387:5868-5873.

[24] Doedel, EJ (2007). AUTO-07P: Continuation and bifurcation software for ordinary differential equations. with major contributions from Champneys, AR, Fairgrieve, TF, Kuznetsov, Yu. A., Oldeman, BE, Paffenroth, RC, Sandstede, B., Wang, XJ, Zhang, C. Available at http://cmvl. cs. concordia. ca/auto.

[25] Ecopath Research and Development Consortium. http://www.ecopath.org/downloads

[26] Ermentrout B (1997). XPPAUT - The Differential Equations Tool.

[27] Fourer R, Gay DM, and Kernighan B (1993). AMPL: a mathematical programming language.

[28] Fryxell JM, Pack C, McCann K, Solberg EJ, and Saether BE (2010). Resource management cycles and the sustainability of harvested wildlife populations. Science 328: 903-906.

[29] Fulton EA. Atlantis. http://atlantis.cmar.csiro.au/. Accessed December 11, 2014.

[30] Gause GF (1934). The struggle for Existence.

[31] Grafton RQ, Kompas T, and Hilborn RW (2007). Economics of overexploitation revisited. Science 318:1601.

[32] Grafton RQ, Kompas T, and Hilborn RW. Limits to the privatization of fishery resources: comment. Land Economics 86:609-613 (2010).

[33] Griffith DR (2008). The ecological implications of individual fishing quotas and harvest cooperatives. Frontiers in Ecology and the Environment 6(4): 191-198.

[34] Hassell, MP (1978). The Dynamics of Arthropod Predator-Prey Systems (Monographs in Population Biology Vol. 13).

[35] Hilborn R (2003). The state of the art in stock assessment: where we are and where we are going. Scentifica Marina 67: S1

[36] Hilborn R (2007). Reinterpreting the state of fisheries and their management. Ecosystems 10: 1362-1369.

[37] Holling, CS (1959). The components of predation as revealed by a study of small mammal predation of the European pine sawfly. Canadian Entomologist 91: 293-320.

[38] Holling, CS (1959) Some characteristics of simple types of predation and parasitism. Canadian Entomologist 91, 385-398.

[39] Holling, CS (1965) The functional response of predators to prey density and its role in mimicry and population regulation. Memoirs of the Entomological Society of Canada 45: 1-60.

[40] Kennedy J (2010). Particle Swarm Optimization. Encyclopedia of Machine Learning: 760-766.

[41] Kuang Y and Beretta E (1998). Global qualitative analysis of a ratio-dependent predator-prey system. Fields Institute Communications 36: 389-406.

[42] Kuznetsov Y(2010). Elements of Applied Bifurcation Theory, Third Edition.

[43] Lotka AJ (1925). The Elements of Physical Biology.

[44] Louisiana Department of Wildlife and Fisheries Office of Fisheries (2011). Oyster Stock Assessment Report of the Public Oyster Area in Louisiana Seed Grounds and Seed Reservations.

[45] National Marine Fisheries Service (2005). Revisions to Guidelines for Assessing Marine Mammal Stocks.

[46] Ostrom E (2006). The value-added of laboratory experiments for the study of institutions and common-pool resources. Journal of Economic Behavior and Organization 61: 149-163.

[47] Perko, LM (1990). Global families of limit cycles of planar analytic systems. Transactions of the American Mathematical Society 322.2: 627-656.

[48] Perko, LM (2001). Differential Equations and Dynamical Systems, Third Edition.

[49] Pinnegar JK, Trenkel VM, and Blanchard JL (2008). 80 years of multispecies fisheries modelling: significant advances and continuing challenges. Advances in Fisheries Science: 50 years on from Beverton and Holt 325-357.

[50] Polking JC. pplane. http://math.rice.edu/ dfield/dfpp.html.

[51] Real, LA (1977). The kinetics of functional response. American Naturalist 111: 289-300.

[52] Rohatgi A. Web Plot Digitizer. http://arohatgi.info/WebPlotDigitizer. Accessed August 22, 2014.

[53] Rosser, JB (2011). Complex Evolutionary Dynamics in Urban-Regional and Ecologic-Economic Systems: From Catastrophe to Chaos and Beyond.

[54] Townsend RE (1992). Bankable individual transferable quotas. Marine Policy 16: 345-348.

[55] Xiao D and Jennings LS (2005). Bifurcations of a ratio-dependent predator-prey system with constant rate harvesting. SIAM Journal on Applied Mathematics 65:737-753.

[56] Xiao D, Li W and Han M (2006). Dynamics in a ratio-dependent predator-prey model with predator harvesting. Journal of Mathematical Analysis and Applications 324:14-29.

[57] Xiao D and Ruan S (2001). Global dynamics of a ratio-dependent predator-prey system. Journal of Mathematical Biology 43:268-290.

[58] Worm B, Hilborn R, Baum JK, Branch TA, Collie JS, Costello C, Fogarty MJ, Fulton EA, Hutchins JA, Jennings S, Jensen OP, Lotze HK, Mace PM, McClanahan TR, Minto C, Palumbi SR, Parma AM, Ricard D, Rosenberg AA, Watson R, Zeller D (2009). Rebuilding Global Fisheries. Science 325: 578-585. Supplemental materials at www.sciencemag.org/cgi/content/full/325/5940/578/DCI

[59] Yasarcan H (2011). Stock management in the presence of significant measurement delays. System Dynamics Review 27: 91-109.

Curriculum Vitae

Michael Crone received a BA in French with a minor in Mathematics from Whitworth College (now Whitworth University) in 1992 and an MS in Mathematics from the University of Wyoming in 1996. Since his previous education, he has worked in education, statistics, and accounting.

He has presented his work at the American Mathematical Society Sectional Meeting in Baltimore in 2014, and the 2012 and 2013 Symposia on Biomathematics and Ecology: Education and Research. He has also given community service presentations to youth on his work in Saint Paul Island, Alaska to various organizations including the Saint Paul School, the Alaska Native Science and Engineering Program and the science camp run by the local tribal government.